RESEARCH ARTICLE

Identifying the molecular target sites for CFTR potentiators GLPG1837 and VX-770

Han-I Yeh[1] , Liming Qiu[2], Yoshiro Sohma[1,3], Katja Conrath[4] , Xiaoqin Zou[2] , and Tzyh-Chang Hwang[1]

The past two decades have witnessed major breakthroughs in developing compounds that target the chloride channel CFTR for the treatment of patients with cystic fibrosis. However, further improvement in affinity and efficacy for these CFTR modulators will require insights into the molecular interactions between CFTR modulators and their binding targets. In this study, we use in silico molecular docking to identify potential binding sites for GLPG1837, a CFTR potentiator that may share a common mechanism and binding site with VX-770, the FDA-approved drug for patients carrying mutations with gating defects. Among the five binding sites predicted by docking, the two top-scoring sites are located at the interface between CFTR's two transmembrane domains: site I consists of D924, N1138, and S1141, and site II$_N$ includes F229, F236, Y304, F312, and F931. Using mutagenesis to probe the importance of these sites for GLPG187 binding, we find that disruption of predicted hydrogen-bonding interactions by mutation of D924 decreases apparent affinity, while hydrophobic amino acids substitutions at N1138 and introduction of positively charged amino acids at S1141 improve the apparent affinity for GLPG1837. Alanine substitutions at Y304, F312, and F931 (site II$_N$) decrease the affinity for GLPG1837, whereas alanine substitutions at F229 and F236 (also site II$_N$), or at residues in the other three lower-scoring sites, have little effect. In addition, current relaxation analysis to assess the apparent dissociation rate of VX-770 yields results consistent with the dose–response experiments for GLPG8137, with the dissociation rate of VX-770 accelerated by D924N, F236A, Y304A, and F312A, but decelerated by N1138L and S1141K mutations. Collectively, these data identify two potential binding sites for GLPG1837 and VX-770 in CFTR. We discuss the pros and cons of evidence for these two loci and the implications for future drug design.

Introduction

Cystic fibrosis (CF), a lethal genetic disease affecting 1 in every 2,500 newborns of Caucasian heritage (Zielenski and Tsui, 1995; Rowe et al., 2005), is a channelopathy caused by malfunction of the chloride channel CFTR (Riordan et al., 1989; Gadsby et al., 2006), whose main physiological function is to transport salt and water across many epithelium-lining organs (Quinton and Reddy, 1991; Bear et al., 1992). Loss-of-function mutations in the *cftr* gene result in multiorgan dysfunction, including chronic lung infection and destruction, the leading cause of morbidity and mortality in CF (Rowe et al., 2005). As a member of the ATP-binding cassette superfamily, CFTR inherits two cytosolic nucleotide-binding domains (NBDs) that exploit the energy of ATP binding and hydrolysis to drive the opening and closing (gating) of an anion-selective pore constructed by its two transmembrane domains (TMDs). In addition, CFTR possesses a unique regulatory domain containing serine/threonine residues for PKA-dependent phosphorylation (Ostedgaard et al., 2001).

Once phosphorylated, CFTR's gating cycle is triggered by ATP-induced NBD dimerization and hydrolysis-elicited separation of NBD dimer (Vergani et al., 2003, 2005; Hwang and Sheppard, 2009; Hwang et al., 2018; Csanády et al., 2019).

Since the first cloning of *cftr* gene (Riordan et al., 1989), ~2,000 different variants (http://www.genet.sickkids.on.ca) have been identified and the disease-associated mutations are classified into six groups based on their molecular mechanisms (Wang et al., 2014; Veit et al., 2016). Both the most prevalent mutation, deletion of phenylalanine at the 508th position (ΔF508), and the third-most common mutation, G551D, are known to impair channel gating (Dalemans et al., 1991; Hwang et al., 1997; Cai et al., 2006; Cui et al., 2006; Bompadre et al., 2007; Miki et al., 2010). Hence, tremendous efforts have been made to develop small molecules known as CFTR potentiators to ameliorate the fundamental defect in CFTR gating (Hwang et al., 1997; Hwang and Sheppard, 1999; Van Goor et al., 2009; Jih et al.,

....
[1]Dalton Cardiovascular Research Center and Department of Medical Pharmacology and Physiology, University of Missouri, Columbia, MO; [2]Dalton Cardiovascular Research Center, Department of Physics and Astronomy, Department of Biochemistry, and Informatics Institute, University of Missouri, Columbia, MO; [3]Department of Pharmaceutical Sciences, School of Pharmacy and Center for Medical Science, International University of Health and Welfare, Tochigi, Japan; [4]Galapagos NV, Mechelen, Belgium.

Correspondence to Tzyh-Chang Hwang: hwangt@health.missouri.edu; Xiaoqin Zou: zoux@missouri.edu.

2017). In 2012, the approval of VX-770, or ivacaftor (*N*-(2,4-di-tert-butyl-5-hydroxyphenyl)-4-oxo-1,4-dihydroquinoline-3-carboxamide), by the U.S. Food and Drug Administration for the treatment of CF patients carrying the G551D mutation ushered in a new era of personalized CF therapeutics. In the following years, VX-770 was approved for the treatment of patients carrying a broader spectrum of CFTR mutants with gating abnormalities (Yu et al., 2012; Van Goor et al., 2014). Despite this revolutionary progress made in the past decade, developing new CFTR potentiators remains an urgent need, as VX-770 is not efficacious enough to completely eliminate the gating defect of G551D (Accurso et al., 2010; Jih and Hwang, 2013; Lin et al., 2016). In addition, VX-770 is shown to pose negative impacts in vitro on the action of VX-809 (Cholon et al., 2014; Veit et al., 2014), a CFTR corrector for mutations that cause trafficking/biogenesis defects such as ΔF508 (Van Goor et al., 2011). While the improved efficacy of second-generation correctors with VX-770 (Davies et al., 2018) and ongoing efforts in discovering new CFTR potentiators (e.g., GLPG1837 or N-(3-carbamoyl-5,5,7,7-tetramethyl-5,7-dihydro-4H-thieno[2,3-c]pyran-2-yl)-lH-pyrazole-5-carboxamide; Van der Plas et al., 2018) promise an encouraging future for CF therapy, the ability to rationally design effective compounds with improved pharmacological properties may hold the key to an ultimate cure of CF.

As VX-770 is a proven prototype of CFTR potentiators, its mechanism of action and potential binding sites may provide the essential insights for the development of next-generation CFTR potentiators. To date, however, the binding site for VX-770 remains unsettled, with several studies proposing different locations, including (1) the interface between the lipid bilayer and TMDs (Jih and Hwang, 2013; Yeh et al., 2015, 2017), (2) a region surrounded by amino acids in between the NBD1/NBD2 interface and the coupling helix 1 (or residue 167–172; Veit et al., 2014), and (3) a binding pocket close to intracellular loop 4 (Byrnes et al., 2018). On the other hand, its mechanism of action can be well described in the context of a gating scheme featuring an energetic coupling between dimerization of the NBDs and opening/closing of CFTR's gate in TMDs (Eckford et al., 2012; Jih and Hwang, 2013). Specifically, by stabilizing the open channel conformations in the TMDs, VX-770 promotes channel opening nearly ubiquitously across a wide spectrum of CFTR mutants (Yu et al., 2012) and works synergistically with other CFTR potentiators with different mechanisms of action, including ATP analogues that target the ATP-binding sites (Aleksandrov et al., 2002; Zhou et al., 2005; Cai et al., 2006; Miki et al., 2010) and 5-nitro-2-(3-phenylpropylamino)benzoate, which appears to promote NBD dimerization (Lin et al., 2016; c.f. Csanády and Töröcsik, 2014).

Recently, we demonstrated that a newly developed CFTR potentiator, GLPG1837, shares the same mechanism of action and a common binding site with VX-770 (Yeh et al., 2017). Based on a classical allosteric modulation model, we further proposed that the two critical properties of a CFTR potentiator, affinity (or potency) and efficacy, can be mathematically defined because of energetic coupling between potentiator binding/unbinding and channel opening/closing. In short, the apparent affinity of a potentiator is determined by how tight it binds to both the open and closed channel conformations, whereas the efficacy is determined by the differences in free energy of binding between the open and closed states, regardless of the absolute value of the free energy of binding in each state. This idea of state-dependent binding demands that the structure of the binding site for a potentiator in an open state should differ from that in a closed state. Thus, in theory, one can manipulate the efficacy and affinity of the potentiator by altering its chemical interactions with the binding sites. However, to realize this ambition of structure-based drug design, one has to first identify the binding sites.

In the past three years, major breakthroughs in solving the atomic structures of zebrafish (zCFTR) and human CFTR (hCFTR) by cryo-EM reveal exquisite chemical features of this protein in different configurations (Zhang and Chen, 2016; Liu et al., 2017; Zhang et al., 2017, 2018b). Taking advantage of the detailed molecular pictures of CFTR and the extensively studied mechanism of action for CFTR potentiators, we envision the structure-based drug design a real possibility once the molecular targets for CFTR potentiators are identified. In this study, our aim is to identify the binding sites for GLPG1837 and VX-770. By combining in silico molecular docking and functional studies using the patch-clamp technique, we identified two potential binding sites, site I and site II_N, for GLPG1837 and VX770 at the interface of CFTR's TMD1 and TMD2. The comparative contribution of these two sites to the binding of CFTR potentiators and the implication of our results for structure-based drug design will be discussed.

Materials and methods

Mutagenesis and channel expression
CFTR mutants were constructed with QuikChange XL kit (Agilent) and sequenced by the DNA Core Facility at the University of Missouri. The CFTR constructs and green fluorescence protein encoding pEGFP-C3 (Takara Bio) were carried by separate pcDNA plasmids and cotransfected with PolyFect transfection reagent (Qiagen) into Chinese hamster ovary cells for all patch-clamp experiments. After transfection, cells were incubated at 27°C for 2–6 d for patch-clamp recordings.

Electrophysiology
In all patch-clamp experiments, the patch pipettes were pulled with a two-stage micropipette puller (PP-81; Narishige) and polished with a homemade microforge to a resistance of 2–5 MΩ in the standard inside-out solution (see chemicals and solution compositions below). Transfected cells grown on a glass chip were transferred to a chamber filled with standard inside-out perfusate on the stage of an inverted microscope (IX51; Olympus) at room temperature. Membrane patches were then excised to an inside-out mode with a seal resistance >40 GΩ. The pipette tip was subsequently positioned at the outlet of a three-barrel perfusion system operated by a fast solution change device (SF-77B; Warner Instruments) with a dead time of ~30 ms (Tsai et al., 2009). The signals were recorded with a patch-clamp amplifier (EPC9; HEKA), filtered at 100 Hz with an eight-pole Bessel filter (LPF-8; Warner Instruments) and digitized to a

Yeh et al.
Binding sites for CFTR potentiators

Journal of General Physiology   913
https://doi.org/10.1085/jgp.201912360

computer at a sampling rate of 500 Hz. The membrane potential was held at −30 mV unless otherwise indicated in the figure legends. Devices that contacted with VX-770 were washed with 50% DMSO after each recording to minimize contamination by residual VX-770 as described previously (Jih and Hwang, 2013).

Chemicals and solution compositions
In all experiments, pipette solution contains (in mM) 140 NMDG-Cl, 2 $MgCl_2$, 5 $CaCl_2$, and 10 HEPES, with pH adjusted to 7.4 by NMDG. The standard inside-out perfusate contains (in mM) 150 NMDG-Cl, 2 $MgCl_2$, 1 $CaCl_2$, 10 EGTA, and 8 Tris, pH 7.4 adjusted with NMDG.

PKA and magnesium ATP (MgATP) were purchased from Sigma-Aldrich and stocked at −20°C. The working concentrations for PKA and MgATP are 25 IU and 2 mM, respectively, unless indicated otherwise in the figures. VX-770 was provided by R. Bridges (Rosalind Franklin University, North Chicago, IL) and stored as a 100 µM stock in DMSO at −70°C. GLPG1837 was provided by Galapagos and stored as a 10 mM stock at −20°C. All chemicals were diluted with the standard inside-out perfusate, and the pH was adjusted to 7.4 with NMDG.

Considering the limited solubility of GLPG1837, we performed the dose–response experiments with a maximum concentration of 40 µM. While this limiting concentration worked well for most of our constructs, some mutations may have resulted in a more drastic shift of the dose–response relationship, and therefore, a complete dose–response curve was not obtained (e.g., Y304A- and Y304T-CFTR).

Electrophysiological data analysis and statistics
Igor Pro 7 (Wave-Metrics) was used to measure the steady-state mean current amplitude, estimate the relaxation time constant, and perform Hill equation fitting with built-in functions to determine the dose–response relationships. The current amplitudes (I) in response to GLPG1837 at different concentrations (µM) were normalized to the amplitudes at 3 µM of GLPG1837 in the same patch by the following equations:

$$\text{normalized response at x µM}$$
$$= \frac{\left(\frac{I(x\ µM\ GLPG1837 + ATP) - I(ATP)}{I(ATP)}\right)}{\left(\frac{I(3\ µM\ GLPG1837 + ATP) - I(ATP)}{I(ATP)}\right)}$$
$$= \frac{I(x\ µM\ GLPG1837 + ATP) - I(ATP)}{I(3\ µM\ GLPG1837 + ATP) - I(ATP)}.$$

The normalized response (y axis) was plotted against the corresponding concentrations (x axis), and Hill equation fitting was performed to estimate the half-effective concentration (EC_{50}). The base of the Hill equation was held at zero, and the maximal response predicted by the Hill equation fitting was normalized to one. Notice that this second normalization is performed for better presentation of the dose–response curves, and it does not affect the value of EC_{50}. The EC_{50} is presented as fitted value ± one standard deviation.

For single-channel studies (Figs. S2 and S4), we decreased the amount of plasmids used for transfection, performed

experiments within 2 d after transfection, and used smaller pipettes (4–5 MΩ) for patch clamping. The membrane potential was held at −30 mV throughout the experiment. CFTR channels were activated by PKA and ATP to a steady state before PKA was removed with the perfusate containing 2 mM ATP. Single-channel traces were inverted for a better visualization. Single-channel kinetic analysis was done with a program developed by Csanády (2000). To ensure the accuracy of the number of functional channels in the patch, we applied GLPG1837 in each experiment to determine the number of channels and analyzed data from patches yielding a maximum of four simultaneous opening steps for microscopic kinetics.

Student's t test was used in Figs. 2 D and S2 B. ANOVA followed by the Dunnett test was used to compare every mean with a control mean in Fig. 6 E; Fig. 8, B and D; Fig. 9 C; and Fig. S3 B. P value < 0.05 was considered statistically significant, and the error bars represent SEM in all figures.

Modeling of the phosphorylated, ATP-bound hCFTR protein
The structure of the phosphorylated, ATP-bound hCFTR was not available at the time when we launched our study. Two high-resolution cryo-EM structures of the whole CFTR protein were solved at the time: the structures of the dephosphorylated, ATP-free hCFTR protein (PDB accession no. 5UAK; Liu et al., 2017) and the phosphorylated, ATP-bound zCFTR protein (PDB accession no. 5W81; Zhang et al., 2017). Both structures were downloaded from the PDB (Berman et al., 2000). Thus, based on the sequence of hCFTR in 5UAK, a homology model of the phosphorylated, ATP-bound hCFTR conformation was built with Modeller (Šali and Blundell, 1993; Fiser et al., 2000; Martí-Renom et al., 2000; Webb and Sali, 2016) using the phosphorylated, ATP-bound zCFTR protein (5W81) as a template. The recommended parameters were adopted and the two bound ATP molecules in 5W81 were included in the modeling work. The output with the lowest value of the MODELLER objective function was selected as the modeled ATP-bound, phosphorylated hCFTR structure, which was used for molecular docking of the ligands, GLPG1837 and VX-770.

Molecular docking
Docking of GLPG1837 and VX-770 onto the CFTR protein was performed through an in-house version of AutoDock Vina (Trott and Olson, 2010), which is capable of outputting a maximum of 500 docking modes (Yan et al., 2016). As compared with the original version, which only provides the top 20 docking modes, our modified version offers a broader view of the docking landscape of our targets. The modeled CFTR protein structure was prepared as described in the last section. The PDB file for the modeled hCFTR protein or the cryo-EM–solved, ATP-bound hCFTR structure was sanitized to retain only the protein structure. The 3-D atomic structures for GLPG1837 and VX-770 were built using the open-source software Avogadro Version 1.2.0 (Hanwell et al., 2012). The PDB files of the CFTR protein and the ligands were converted to the PDBQT format (Forli et al., 2016), which is specific for the AutoDock Vina. Through the conversion process, partial charges were calculated by the AutoDock Vina with the Gasteiger method and assigned to the atoms of the protein, and the nonpolar hydrogen atoms were united with the

heavy atoms to which they were bonded. In docking, the protein structure was treated as a rigid body, whereas the ligands were allowed to be flexible. The docking results targeting the TMDs of the hCFTR were ranked from the best to the worst according to their docking energy scores. The more negative the energy score, the better the rank of the binding mode.

Online supplemental material

Fig. S1 provides the chemical structures and docking modes for GLPG1837 and VX-770 in the cryo-EM structure of phosphorylated, ATP-bound hCFTR. Fig. S2 presents microscopic recordings of F312A-CFTR. Fig. S3 demonstrates the response of site IV mutants to the addition/removal of VX-770. Fig. S4 shows microscopic recordings of Y304A- and Y304F-CFTR. Figs. S5 and S6 show the effects of GLPG1837 on zCFTR and R347D/D924R hCFTR, respectively.

Results

Finding the binding sites of GLPG1837 and VX-770 via molecular docking

We recently demonstrated that the CFTR potentiators GLPG1837 and VX-770 share a common mechanism of action as well as a common binding site (Yeh et al., 2017). In this study, our goal was to identify their exact binding sites in the CFTR protein. As a first step to hunt for the potential binding modes, we performed a docking calculation of GLPG1837 by running the AutoDock Vina program on a hCFTR homology model (see details in Materials and methods). This homology model was built mainly using the template structure of the phosphorylated and ATP-bound zCFTR (Zhang et al., 2017), which represents a channel closest to an open configuration among the available atomic structures at the time when we launched this project.

Our docking was specifically focused on CFTR's TMDs, where the binding sites for both GLPG1837 and VX-770 are presumably located (Jih and Hwang, 2013; Yeh et al., 2015, 2017). The output poses of GLPG1837 were clustered visually, and the pose exhibiting most interactions with CFTR was selected as the representative conformation for each site. These poses and the corresponding sites were numbered according to their energy scores (–8.8, –8.2, –7.8, and –7.7, respectively) and are shown in Fig. 1 A. The expanded views of each site, labeled as site I, II, III, and IV, are displayed in Fig. 1, B–E. We caution our readers that due to the limited accuracy of the existing docking scoring functions (Grinter and Zou, 2014; Gaieb et al., 2019), the small differences in these energy scores should not be used to determine the rankings of these poses; mutations and functional studies are required to verify these potential binding sites. Nonetheless, the docking methodology does provide a blunt yet valuable screening tool to preselect otherwise innumerable potential binding sites for functional studies.

A two-dimensional chemical structure of GLPG1837 can be found in Fig. S1 A. In the predicted binding sites, we first identified the amino acid residues that have any atoms within 5 Å of GLPG1837. Among these residues, we then defined the ones that have a side chain pointing toward the bound ligand and thus can potentially interact with GLPG1837 as the

candidates for further examination with the patch-clamp functional assay. The predicted binding sites were then tested by first making mutations at the above-identified positions and then measuring CFTR currents at different potentiator concentrations with the patch-clamp technique to quantitatively assess the effects of mutations in each binding site on the dose–response relationships of GLPG1837.

This straightforward assay, however, is impractical for VX-770, since we have previously determined that 200 nM is already a saturating concentration for VX-770, and the actual EC_{50} may be much lower (Jih and Hwang, 2013; but compare Hadida et al., 2014; Van Goor et al., 2014). As concentrations in the range of picomolars must be used to complete the dose–response curve for VX-770, it will take very long time to achieve a steady state. In addition, the stickiness of VX-770 to the recording device also adds another level of technical difficulty in assuring the correct concentrations used in each experiment. Therefore, we used GLPG1837, which assumes a micromolar affinity and is readily removed from the system, in all the following dose–response experiments and took a different strategy to estimate the affinity for VX-770, as described latter in this section.

Three amino acids (D924, N1138, and S1141) in site I contribute to the binding of GLPG1837

The top-scoring site I consists of three amino acids (D924, N1138, and S1141) located at the interfaces between CFTR's two TMDs (Fig. 1 B). We started with D924 to test whether site I is a potential binding site for GLPG1837. In this binding mode, the aspartate side chain appears to be hydrogen bonded with the two nitrogen atoms in the pyrazole ring of GLPG1837. We reasoned that the binding affinity of GLPG1837 may be changed by introducing mutation to disrupt the hydrogen bonding. Fig. 2 shows the effects of mutations at D924 on the apparent affinity for GLPG1837. As shown in Fig. 2 A, while the pre-phosphorylated WT-CFTR currents can be potentiated by GLPG1837 at a saturating concentration of 3 µM in the continuous presence of ATP, an application of 20 µM GLPG1837 further enhances the currents of D924N-CFTR, indicating a rightward shift of the dose–response relationship or an increase in EC_{50}. We next replaced the aspartate with alanine (D924A) in an attempt to observe a more drastic change in the affinity of GLPG1837. Although a steady-state dose–response relationship and a corresponding EC_{50} cannot be attained because we could not obtain macroscopic currents for D924A-CFTR (but a representative microscopic recording is shown in Fig. 2 B), we can safely conclude that the apparent affinity of D924A-CFTR for GLPG1837 is decreased by ≥10-fold (EC_{50} = 0.26 µM for WT-CFTR) based on two observations. First, we barely discerned any potentiating effects on D924A-CFTR at 3 µM GLPG1837, which was the saturating concentration for WT-CFTR. Second, upon changing the [GLPG1837] from 20 µM to 3 µM, the channel activity immediately decreased to the level comparable to the activity in the absence of GLPG1837, suggesting a rapid dissociation of GLPG1837 from D924A-CFTR. These two observations indicate that the EC_{50} of D924A-CFTR should be >3 µM. Fig. 2 C summarized the dose–response curves for WT-, D924E-, and D924N-CFTR. Of note, the EC_{50} of the charge-conserving mutant
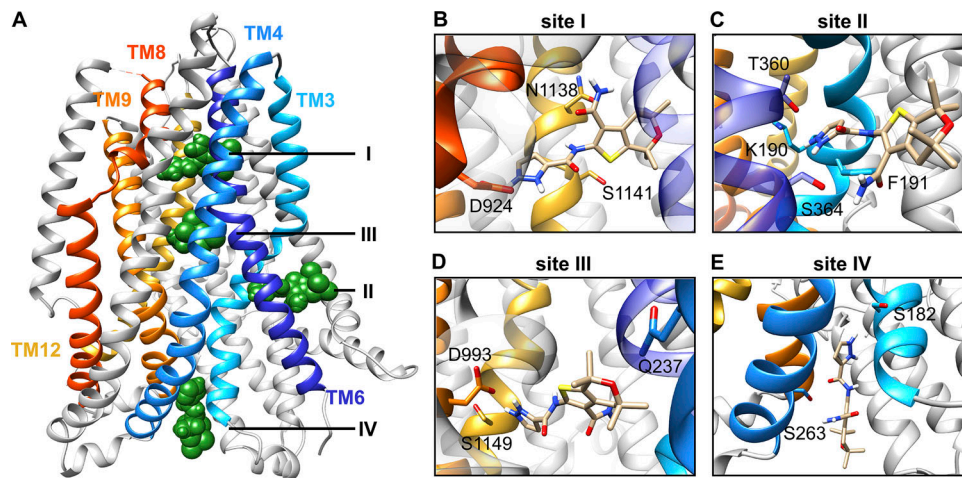
Figure 1. **Four potential binding sites (I–IV) for GLPG1837 predicted by molecular docking. (A)** The docking modes of GLPG1837 (in ball representation and colored green) at sites I–IV in the transmembrane domains of a homology model of hCFTR. The transmembrane segments involved in constructing the binding sites are colored. The four binding sites are ranked according to the most negative (site I) to the least negative (site IV) docking energy scores. The more negative the energy scores are, the tighter the binding is. **(B–E)** Expanded views of sites I–IV. GLPG1837 and the individual amino acids forming each binding site are shown in the stick representation and are colored by element (C, gold; N, blue; O, red; S, yellow). The amino acid residues subjected to further investigation with the patch-clamp technique are listed below with their residing TM in parentheses. Site I: D924 (TM8), N1138 (TM12), and S1141 (TM12). Site II: K190 (TM3), F191 (TM3), T360 (TM6), and S364 (TM6). Site III: Q237 (TM4), D993 (TM9), and S1149 (TM12). Site IV: S182 (TM3) and S263 (TM4).

D924E-CFTR, which preserves the negative charge at this position, is slightly different from that of WT-CFTR. These side-chain–dependent incremental changes of EC_{50} among D924E, D924N, and D924A mutations support the idea that D924 is involved in the binding of GLPG1837.

While the dose-response experiment is a straightforward assay to obtain the apparent affinity, one can also measure the apparent dissociation rate (or the off-rate) of the drug by monitoring the time course of current decay upon sudden removal of the compound. In Fig. 2 A, the current decay upon removal of 3 µM GLPG1837 can be fitted with a single exponential function, yielding a time constant of 24.4 s for WT-CFTR and 3.8 s for D924N-CFTR, respectively. The statistical

comparison shown in Fig. 2 D confirms a faster dissociation of GLPG1837 (i.e., shorter relaxation time constant) from D924N-CFTR, which is consistent with a lower apparent affinity seen in the dose–response relationships (Fig. 2 C). It should be noted that the affinity of a drug is determined by both its on-rate and off-rate, and this relaxation analysis only assesses the off-rate. Despite this caveat, this measurement can be used as a complementary tool to evaluate any changes in the binding affinity of a molecule when performing dose–response experiment is not feasible, as in the case of VX-770 (see Figs. 8 and 9 below).

The next amino acid in site I is N1138 in transmembrane segment (TM) 12. Interestingly, the side chain of N1138 resides close to the hydrophobic region of GLPG1837. We thus
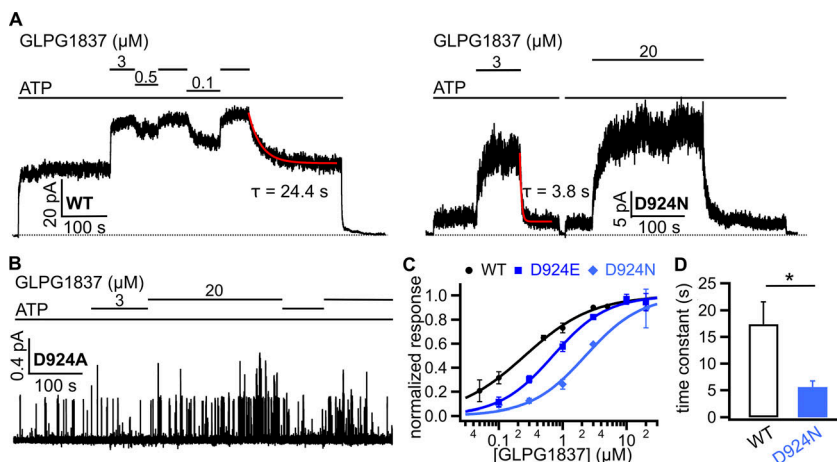
Figure 2. **Mutations of the D924 residue decrease the apparent affinity for GLPG1837. (A)** Real-time recordings of macroscopic WT-CFTR (left) and D924N-CFTR (right) currents in response to various concentrations of GLPG1837. In the continuous presence of 2 mM ATP, different concentrations of GLPG1837 were applied to the channels preactivated with PKA plus ATP at a holding potential of −30 mV. The current decay following the removal of 3 µM GLPG1837 was fitted with a single-exponential function (red curve) to yield a relaxation time constant (τ). **(B)** Effects of GLPG1837 on the activity of D924A-CFTR channels. The activity in the presence of 3 µM GLPG1837 remained similar to the basal activity at 2 mM ATP. The increased activity at 20 µM GLPG1837 rapidly disappeared upon changing [GLPG1837] back to 3 µM, indicating a fast dissociation of GLPG1837. The membrane potential was held at −50 mV to better discern the single-channel opening events. **(C)** A graded rightward shift of the dose–response relationships for D924E- and D924N-CFTR. EC_{50} (µM): 0.26 ± 0.04 (WT), 0.71 ± 0.07 (D924E), and 2.29 ± 0.78 (D924N). Each data point represents mean values from three to seven patches. **(D)** Current relaxation time constants upon removal of GLPG1837 for WT- and D924N-CFTR. τ_{WT} = 17.4 ± 4.2 s (n = 5); τ_{D924N} = 5.6 ± 1.1 s (n = 6). *, P < 0.05 (Student's t test). Error bars represent SEM.
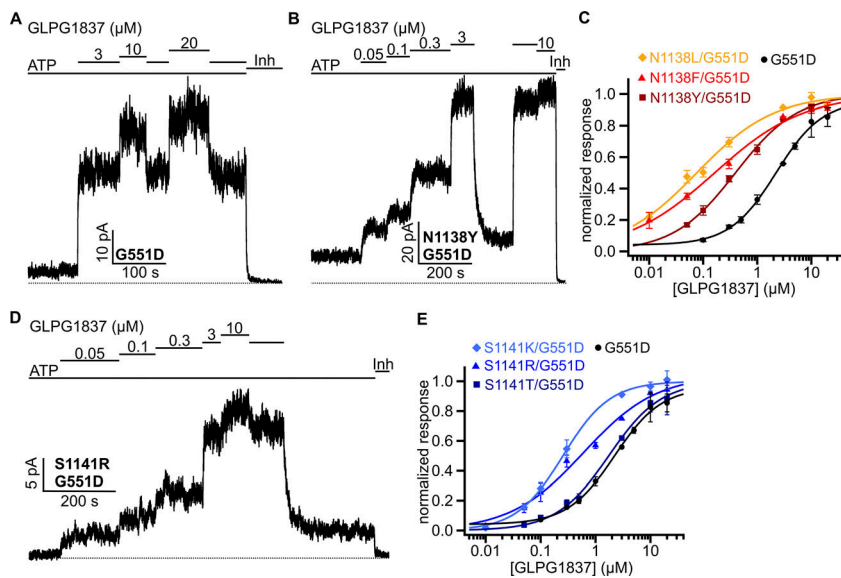
Figure 3. **Increase in the apparent affinity for GLPG1837 by mutations at residue N1138 and S1141 in G551D-CFTR. (A and B)** Representative recordings of G551D-CFTR (A) and N1138Y/G551D-CFTR (B) in response to GLPG1837. The macroscopic currents in the continuous presence of ATP increased with application of GLPG1837 in a dose-dependent manner. 5 μM CFTR$_{inh}$-172 (Inh) was applied at the end of the recording to attain the baseline. **(C)** Dose–response relationships of GLPG1837 for channels with a second mutation (N1138L, N1138F, or N1138Y) introduced into the G551D background. The leftward shift of the three double mutants suggests an increase in the apparent affinity for GLPG1837. EC$_{50}$ (μM): 2.19 ± 0.33 (G551D), 0.08 ± 0.02 (N1138L/G551D), 0.16 ± 0.05 (N1138F/G551D), and 0.40 ± 0.10 (N1138Y/G551D). **(D)** A representative trace for the dose-dependent increase in S1141R/G551D-CFTR currents by GLPG1837. **(E)** Dose–response relationships of GLPG1837 for S1141K/G551D-, S1141R/G551D-, and S1141T/G551D-CFTR. The apparent affinity for GLPG1837 is increased by S1141K and S1141R mutations, while the S1141T mutation poses little effect. EC$_{50}$ (μM): 0.26 ± 0.02 (S1141K/G551D), 0.51 ± 0.13 (S1141R/G551D), and 1.74 ± 0.31 (S1141T/G551D). Each data point in C and E represents mean values of the normalized response to GLPG1837 determined from three to eight patches. Error bars represent SEM.

speculated that substitutions of N1138 with hydrophobic amino acids may actually improve the binding of GLPG1837. To test this idea, we chose G551D-CFTR as the background for two reasons. First, due to its intrinsic low open probability (P$_o$; Bompadre et al., 2007; Lin et al., 2014), the maximal fold increase of G551D-CFTR currents in response to GLPG1837 is 20-fold greater than that of WT-CFTR (Yeh et al., 2017), which allows us to clearly observe the stepwise changes in current amplitudes at different concentrations of GLPG1837 (Fig. 3 A). Second, since the apparent affinity for GLPG1837 on G551D-CFTR is 10-fold lower than that on WT-CFTR mostly due to state-dependent binding (Yeh et al., 2017), it leaves a potentially larger room for the affinity to be increased. Fig. 3 B shows a representative recording of the dose-dependent change in N1138Y/G551D-CFTR currents in response to GLPG1837. A similar protocol was used to obtain the dose–response relationships for GLPG1837 on N1138F/ and N1138L/G551D-CFTR. In Fig. 3 C, the dose–response curves for these three mutants are leftward shifted compared with G551D-CFTR, supporting the hypothesis that hydrophobic amino acids substitutions at N1138 enhance binding of GLPG1837 (see Discussion for more details).

As seen in the docking mode shown in Fig. 1 B, the side chain of S1141 is ~3 Å away from the thiophene ring of GLPG1837. Compared with N1138, S1141 is somewhat distant from the bound drug, suggesting a weaker interaction. One maneuver that may enhance its interaction is to convert S1141 to a positively charged amino acid to take advantage of a possible cation–π electron interaction. We therefore altered S1141 to lysine or arginine in the G551D background and determined the dose–response relationships for the double mutants S1141K/G551D-CFTR and S1141R/G551D-CFTR. Indeed, a leftward shift was observed, whereas the threonine substitution, which carries a hydroxyl group like serine, poses minimal effect (Fig. 3, D and E).

To this point, we found that mutations on the three residues in site I either decrease (D924) or increase (N1138 and S1141) the affinity for GLPG1837, supporting the notion that these amino acids may contribute to the binding of GLPG1837.

Alanine substitution on residues in site II, III, and IV has little impact on the affinity for GLPG1837

We next tested the effect of alanine substitution on the amino acids in the three lower-scoring sites (II, III, and IV) predicted by docking. Again, we reasoned that if any of the residues were involved in the binding of GLPG1837, substitution of the original side chain with alanine should disrupt the drug–protein interaction and hence decrease the affinity. Fig. 4 summarizes the dose–response relationships for mutations in site II, III, and IV. Site II consists of three hydrophilic amino acids in CFTR's TM3 and TM6, namely K190 (TM3), T360 (TM6), and S364 (TM6), and a phenylalanine (F191) in TM3. Replacing the former three residues with alanine poses minimal effect on the affinity for GLPG1837 (Fig. 4, A and B), as the dose–response curves show little shift. We were not able to assess the effect of F191A mutation, as F191A-CFTR failed to generate detectable currents in our experimental setting. Similarly, we tested all three residues in site III, including Q237 in TM4, D993 in TM9, and S1149 in TM12. While the dose–response curves for D993A-CFTR and S1149A-CFTR are very close to that for WT-CFTR (Fig. 4 D), Q237A-CFTR appears to decrease the affinity and shift the curve rightward (Fig. 4, C and D). However, it should be noted that this slight change in apparent affinity could be attributed to a decreased P$_o$ of this mutant based on the idea of state-dependent binding (Yeh et al., 2017). The clue for a lower P$_o$ is that the maximal percent increase of Q237A-CFTR currents potentiated by GLPG1837 (615%; Table 1) is much larger than that of WT-CFTR
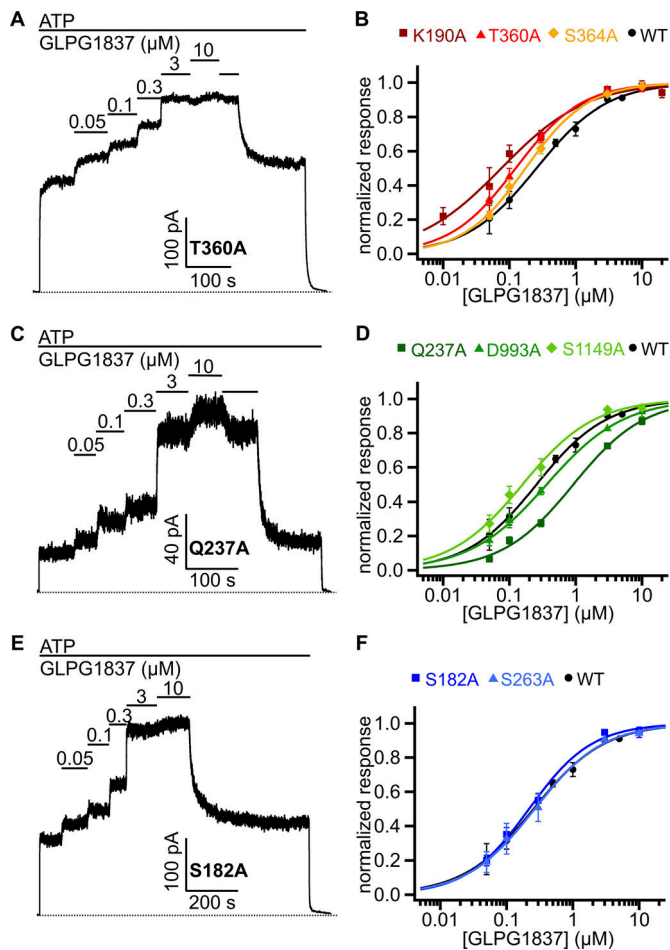
Figure 4. **Effects of alanine substitutions at residues in site II, III, and IV on the apparent affinity for GLPG1837. (A)** A representative trace showing the dose-dependent increase in T360A-CFTR currents. T360A is unlikely to decrease the apparent affinity for GLPG1837 as, like WT-CFTR, the currents saturate at 3 µM of GLPG1837. **(B)** Dose–response relationships of GLPG1837 for CFTR mutants in site II. EC_{50} (µM): 0.08 ± 0.01 (K190A), 0.12 ± 0.01 (T360A), 0.18 ± 0.01 (S364A), and 0.26 ± 0.04 (WT). **(C)** Concentration-dependent response of Q237A-CFTR currents to GLPG1837. **(D)** Summary of dose–response curves of GLP1837 for CFTR mutants in site III. While D993A-CFTR and S1149A-CFTR have an EC_{50} close to WT-CFTR, Q237A-CFTR decreases the apparent affinity for GLPG1837, reflecting by the rightward shift in the dose–response curve. EC_{50} (µM): 0.92 ± 0.32 (Q237A), 0.36 ± 0.04 (D993A), and 0.16 ± 0.03 (S1149A). **(E)** A macroscopic recording showing the effects of GLPG1837 on S182A-CFTR. **(F)** The dose–response relationships of GLPG1837 for site IV mutants, S182A- and S263A-CFTR. Both mutations have little effect on the apparent affinity for GLPG1837, as their dose–response curves virtually overlap with the curve for WT-CFTR. EC_{50} (µM): 0.22 ± 0.04 (S182A) and 0.27 ± 0.05 (S263A). Each data point in B, D, and F is the mean values determined from three to five patches. Error bars represent SEM.

(115%; Table 1). A simple calculation yields a maximum P_o of 0.14 (1/7.15) for Q237A-CFTR (vs. ~0.4 for WT).

The site with the lowest score or least negative binding energy (IV) has two serine residues located within 5 Å of the bound GLPG1837, namely S182 in TM3 and S263 in TM4. Similar to the results for site II and site III, alanine substitution of either of these two serines has little effect on the dose–response relationships of GLPG1837 (Fig. 4, E and F). The dose–response curves for S182A-CFTR and S263A-CFTR almost overlap with

that for WT-CFTR, suggesting that neither amino acid is involved in the binding of GLPG1837.

A new binding site, II_N, revealed in the lately solved hCFTR atomic structure

By combining in silico docking and the functional assay, we identified site I as a likely binding site for the CFTR potentiator GLPG1837. However, one caveat in the aforementioned study is that the docking simulation was based on a homology model, which could be different significantly from the actual structure of hCFTR. Fortunately, the atomic structure of the ATP-bound, phosphorylated hCFTR was solved with cryo-EM in late 2018 (Zhang et al., 2018b). We immediately performed molecular docking on this structure and compared the results with those shown in Fig. 1. While both GLPG1837 and VX-770 could be docked to the same four binding sites in this new cryo-EM structure (Fig. S1, A–D), an additional binding site located at the interface between TM4, TM5, and TM8 was identified (Fig. 5 A; and Fig. S1, E and F). This new site (named site II_N, because its score is between site I and II) consists of four phenylalanine (F229, F236, F312, and F931) residues and one tyrosine (Y304) residue, forming a hydrophobic cradle to accommodate the potentiators (Fig. 5 B). This binding pocket was not found in our homology model, because the side chain of residue F931 in the original zCFTR structure (PDB accession no. 5W81) protrudes in a direction that clashes with the potentiators. As both GLPG1837 and VX-770 are hydrophobic molecules carrying multiple rings (Van Goor et al., 2009; Van der Plas et al., 2018), we speculated that ring–ring stacking interactions could play an important role in stabilizing drug binding. To test this idea, we determined the dose–response relationships for GLPG1837 with each residue replaced with alanine one at a time. Among the five residues identified in site II_N, alanine substitution at Y304 and F931 decreases the apparent affinity for GLPG1837 (Fig. 6, A and B), whereas F229A and F236A have little effect (Fig. 6 B). The EC_{50} for F312A appears to be similar to that for WT-CFTR, but the efficacy (i.e., maximal percent increase of currents) is reduced from 115% in WT-CFTR to 26% for F312A-CFTR (Table 1), suggesting that F312A may increase the P_o. According to the idea of state-dependent binding (Yeh et al., 2017), the apparent affinity should increase as the P_o increases. The fact that F312A-CFTR may bear a higher P_o but unchanged EC_{50} implies its actual affinity for GLPG1837 is reduced. This idea will be tested in Fig. 7 below.

Y304 is in close proximity to the pyrazole group of GLPG1837, where both the hydroxyl group and aromatic ring of Y304 could potentially interact with GLPG1837. We substituted Y304 with phenylalanine, threonine, and alanine. Fig. 6 C shows a representative recording of Y304F-CFTR in response to GLPG1837, and the dose–response relationship yields an EC_{50} of 2.28 ± 0.34 µM (Fig. 6 D). Y304T-CFTR, which preserves the hydroxyl group, also exhibits a decreased affinity. As the currents of Y304T-CFTR at 3 µM GLPG1837 are still <50% of that with 30 µM GLPG1837, the highest concentration applied in the experiments, the EC_{50} for Y304T-CFTR is expected to be >3 µM. Similar results were observed with Y304A-CFTR. These data suggest a major role of the side chain of Y304 in the binding of GLPG1837.

Table 1. EC$_{50}$, ΔΔG, efficacy for GLPG1837, and relaxation time constants for the addition and removal of VX-770 for mutations in the five predicted binding sites

	EC$_{50}$ (µM)	ΔΔG (kJ/mol)	Efficacy (% increase)	τ_{on} (VX-770) (s)	τ_{off} (VX-770) (s)
WT	0.26 ± 0.04	–	115 ± 7	6.7 ± 1.2	361 ± 39
G551D	2.19 ± 0.33	–	4,115 ± 714	5.9 ± 2.4	68 ± 14
Site I					
D924A	>3	<−6.06	–	–	–
D924E	0.71 ± 0.07	−2.49	194 ± 8	–	–
D924N	2.29 ± 0.78	−5.39	464 ± 73	78 ± 18	115 ± 7
N1138F/G551D	0.16 ± 0.05	6.48	666 ± 131	–	–
N1138L/G551D	0.08 ± 0.02	8.20	253 ± 32	18 ± 5	268 ± 25
N1138Y/G551D	0.40 ± 0.10	4.21	1,106 ± 279	–	–
S1141K/G551D	0.26 ± 0.02	5.28	1,326 ± 161	14 ± 6	221 ± 50
S1141R/G551D	0.51 ± 0.13	3.61	2,868 ± 479	–	–
S1141T/G551D	1.74 ± 0.31	0.57	2,167 ± 329	–	–
Site II$_N$					
F229A	0.46 ± 0.07	−1.41	135 ± 26	6.2 ± 1.3	338 ± 49
F236A	0.34 ± 0.14	-0.67	81 ± 14	19 ± 8	173 ± 45
Y304A	>3	<−6.06	>80 ± 9	49 ± 11	18 ± 6
Y304F	2.28 ± 0.34	−5.38	82 ± 12	–	–
Y304T	>3	<−6.06	>101 ± 7	–	–
F312A (2 mM ATP)	0.40 ± 0.13	−1.07	26 ± 2	–	–
F312A (30 µM ATP)	1.30 ± 0.26	−3.99	105 ± 12	15 ± 1	38 ± 5
F931A	1.14 ± 0.26	−3.57	83 ± 12	–	–
Site II				–	–
K190A	0.08 ± 0.01	2.92	61 ± 12	–	–
T360A	0.12 ± 0.01	1.92	120 ± 38	–	–
S364A	0.18 ± 0.01	−0.91	126 ± 5	–	–
Site III				–	–
Q237A	0.92 ± 0.32	−3.13	615 ± 101	–	–
D993A	0.36 ± 0.04	−0.81	283 ± 47	–	–
S1149A	0.16 ± 0.03	1.20	139 ± 36	–	–
Site IV					
S182A	0.22 ± 0.04	0.41	138 ± 23	8.2 ± 1.5	343 ± 96
S263A	0.27 ± 0.05	−0.09	148 ± 18	6.1 ± 1.5	288 ± 68

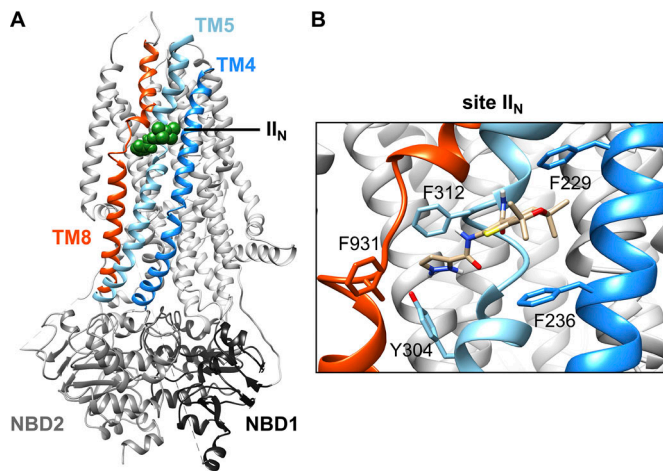ΔΔG was calculated from the following equation: $\Delta G_{(mutant)} - \Delta G_{(WT)} = \Delta\Delta G = -RT\ln\frac{EC_{50(mutant)}}{EC_{50(WT)}}$.
EC$_{50(WT)}$ was replaced with EC$_{50(G551D)}$ when the mutation was introduced to G551D-CFTR background.

Although for technical reasons (see Materials and methods) we did not obtain a complete dose–response relationship of GLPG1837 for Y304A- and Y304T-CFTR, the current relaxation analysis upon removal of GLPG1837, which reflects the apparent dissociation rate, did provide another line of supporting evidence for a significant decrease in the affinity (Fig. 6 E). Both Y304A- and Y304T-CFTR shorten the relaxation time constant to <5 s (c.f., ~17 s for WT-CFTR).

As briefly mentioned above, although F312A in site II$_N$ appears to have little impact on the EC$_{50}$ of GLPG1837 (Fig. 6 B), the

true binding affinity for GLPG1837 in F312A-CFTR may be much lower when we take the effects of state-dependent binding into consideration. Fig. 7 A shows a real-time recording of F312A-CFTR currents in response to GLPG1837 in the presence of 2 mM ATP. The maximally potentiated currents at 20 µM GLPG1837 are only ~1.3-fold of the initial currents in the presence of ATP, implying that the P$_o$ of F312A-CFTR could be greater than WT-CFTR, which responds to GLPG1837 with twofold increase in macroscopic currents (Fig. 2). Indeed, single-channel kinetic analysis confirmed that the P$_o$ of F312A-CFTR (0.63 ± 0.04; Fig.

Yeh et al.
Binding sites for CFTR potentiators

Journal of General Physiology
https://doi.org/10.1085/jgp.201912360

919

Figure 5. **A new site (site II$_N$) for GLPG1837 found in the transmembrane domains of phosphorylated, ATP-bound hCFTR. (A)** Cryo-EM structure of phosphorylated, ATP-bound hCFTR featuring a new site (site II$_N$) for GLPG1837 (colored green with ball representation) identified by docking (NBD1, black; NBD2, gray). **(B)** An expanded view of site II$_N$. The five amino acid residues within 5 Å of GLPG1837, including F229 (TM4), F236 (TM4), Y304 (TM5), F312 (TM5), and F931 (TM8), appear to form a hydrophobic pocket for the bound ligand. The GLPG1837 is colored by element, and the side chains of the five amino acids are shown in the stick representation.

S2) is higher than the P$_o$ of WT-CFTR mainly due to a prolonged open time constant (∼0.4, Zhou et al., 2006; Yeh et al., 2017).

According to the idea of state-dependent binding, the positive correlation between apparent affinity and P$_o$ demands that the measured apparent affinity increases as the P$_o$ increases (Yeh et al., 2017). Thus, the observation that the measured EC$_{50}$ for GLPG1837 in F312A-CFTR is slightly higher than that of WT-CFTR (0.4 vs. 0.26 µM) suggests a much lower affinity for GLPG1837 than WT-CFTR. In other words, the true binding affinity for GLPG1837 is significantly decreased by the F312A

mutation, but the effect is masked by the opposing effect of its high P$_o$. This idea can be further examined simply by adjusting the P$_o$ of F312A-CFTR to the level of WT-CFTR by lowering the concentration of ATP. In Fig. 7 B, the currents of F312A-CFTR are decreased by 45 ± 3% with 30 µM ATP compared with the initial currents at 2 mM ATP (n = 7), reducing the P$_o$ to ∼0.35 (0.63 × 55% = 0.35). In this condition, the dose–response relationship is rightward shifted, and Hill equation fitting yields an EC$_{50}$ of 1.30 ± 0.26 µM (Fig. 7 C). Of note, for WT-CFTR, a 20-fold reduction of the P$_o$ to 0.02 only increases the EC$_{50}$ from 0.26 to 1.7 µM (Yeh et al., 2017), suggesting that an EC$_{50}$ of 1.3 µM at a P$_o$ of 0.35 in F312A-CFTR is unlikely accounted for simply by a state-dependent binding mechanism. We thus conclude that alanine substitution of F312 indeed reduces the apparent affinity for GLPG1837, supporting the notion that F312 contributes to binding of GLPG1837.

The affinity for VX-770 is altered by mutations in site I and site II$_N$

So far, we narrowed down the potential binding sites for GLPG1837 to two loci, site I and site II$_N$. As discussed earlier, it is impractical, at least in our experimental setting, to perform the same dose–response experiments for VX-770 to confirm whether it binds to the same sites. Here, we took the alternative strategy of relaxation analysis described in Fig. 2 D, in which the reduced affinity of GLPG1837 is reflected by a faster current decay upon its removal, implicating a faster dissociation rate. Fig. 8, A and B show the current relaxation upon removal of VX-770 in WT-CFTR and D924N-CFTR. While the WT-CFTR currents relaxed back to the initial level with a time constant of 361 ± 39 s, D924N shortened the relaxation time constant to 115 ± 7 s (P < 0.05). The accelerated dissociation of VX-770 in D924N-CFTR is consistent with our observation for GLPG1837 in Fig. 2 D and supports the hypothesis that D924 is involved in the binding of both VX-770 and GLPG1837. Next, we tested whether the
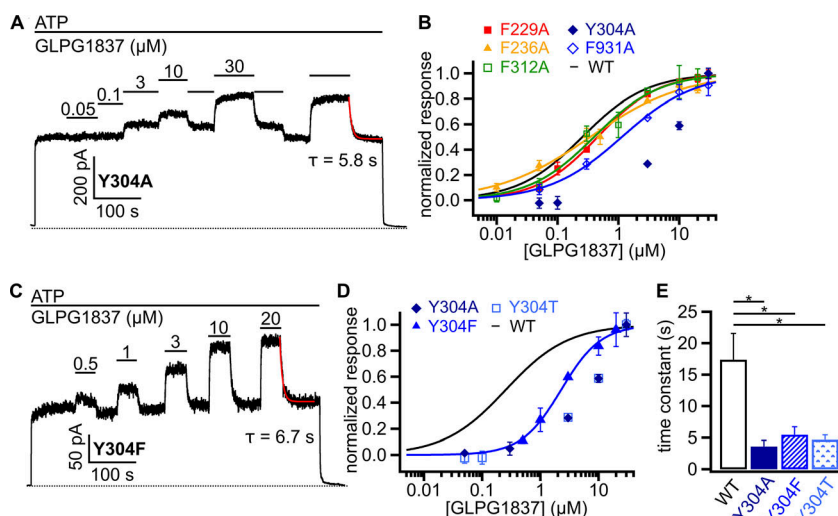
Figure 6. **Dose–response relationships for CFTR mutants in site II$_N$. (A)** A representative recording of Y304A-CFTR in response to GLPG1837. The relaxation time course upon removal of GLPG1837 can be fitted with a single-exponential function (red curve), yielding a time constant of 5.8 s. **(B)** Summary of the dose–response curves for five CFTR mutants with alanine substitution in site II$_N$. Notice that the currents of Y304A-CFTR have not saturated with 30 µM GLPG1837, and thus, fitting with the Hill equation was not performed. The black curve is the fitted dose–response relationship for WT-CFTR from Fig. 2 C. EC$_{50}$ (µM): 0.46 ± 0.07 (F229A, red), 0.34 ± 0.14 (F236A, yellow), 0.40 ± 0.13 (F312A, green), and 1.14 ± 0.26 (F931A, blue). **(C)** Dose-dependent increase of Y304F-CFTR currents at various [GLPG1837]. The relaxation time constant for the removal of GLPG1837 (red curve) is 6.7 s. **(D)** Dose–response relationships for mutations at Y304. EC$_{50}$ for Y304F-CFTR is 2.28 ± 0.34 µM. **(E)** Decrease in relaxation time constants upon removal of GLPG1837 in Y304A/F/T-CFTR. Time constants: 17.4 ± 4.2 s (WT), 3.6 ± 1.0 s (Y304A), 5.5 ± 1.3 s (Y304F), and 4.7 ± 0.8 s (Y304T). n = 5. *, P < 0.05 (ANOVA followed by Dunnett test). Error bars represent SEM.
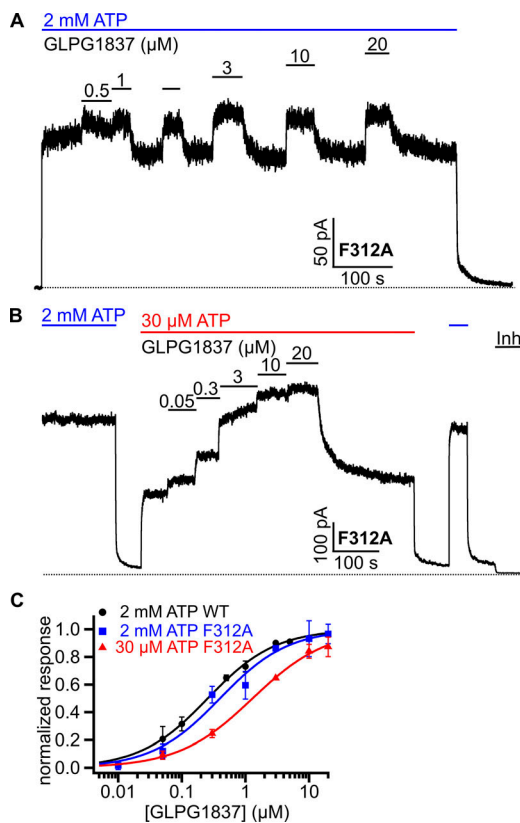
Figure 7. **Effects of the F312A mutation on the apparent affinity for GLPG1837. (A)** Dose-dependent increase of F312A-CFTR currents by GLPG1837 in the presence of 2 mM ATP. The activity of F312A-CFTR at 2 mM ATP can be further potentiated by GLPG1837 with a saturating concentration of 3 µM. Note the much-reduced efficacy of GLPG1837 (26 ± 2% increase of the currents, $n = 7$) compared with that of WT-CFTR (115 ± 7% increase, $n = 19$), suggesting an increase of the P_o by the F312 mutation. **(B)** Dose-dependent increase of F312A-CFTR currents at 30 µM ATP. The application of 30 µM ATP (red) reduced the currents by half compared with the initial currents at 2 mM ATP (blue). In the presence of 30 µM ATP, different concentrations of GLPG1837 were applied to attain the dose–response relationship, and a larger efficacy of GLPG1837 was seen. After washout of GLPG1837 and subsequent removal of 30 µM ATP, 2 mM ATP was applied to ensure the same level of activity compared with the initial activity at the beginning of the recording. 5 µM $CFTR_{inh}$-172 (Inh) was added at the end to observe the baseline. **(C)** Dose–response relationships of GLPG1837 for F312A-CFTR in the presence of 2 mM or 30 µM ATP. With 30 µM ATP, F312A-CFTR has a P_o comparable to WT-CFTR, and the rightwardly shifted dose–response curve indicates an actual decrease in the apparent affinity for GLPG1837. EC_{50} (µM): 0.26 ± 0.04 (WT), 0.40 ± 0.13 (F312A, 2 mM ATP), and 1.30 ± 0.26 (F312A, 30 µM ATP). Each data point at different [GLPG1837] represents mean values from three to seven patches. Error bars represent SEM.

other two residues in site I, N1138 and S1141 (in the G551D background), also contribute to the binding of VX-770 in a manner similar to their interaction with GLPG1837. In Fig. 8, C and D, single-exponential fitting yields a time constant of 68 ± 14 s for the currents decay upon removal of VX-770 in G551D-CFTR, whereas the relaxation time constant is prolonged to 221 ± 50 s for S1141K/G551D-CFTR (P < 0.05) and 268 ± 25 s for N1138L/G551D (P < 0.05). It should be noted that the effect of VX-770 cannot be washed out completely within the

experimentally permissible time, which is likely due to its extremely high affinity and "stickiness" to the recording system (Jih and Hwang, 2013; Yeh et al., 2015, 2017). As the currents do not relax back to the initial level before the application of VX-770 (Fig. 8, A and C), the value of the relaxation time constant is likely to be somewhat underestimated. Nevertheless, some observed changes in the decay time constants are visually discernible (e.g., Fig. 8 and also see Fig. 9 below) and hence support the notion that mutations in site I change the affinity for VX-770.

While the decay time constant reflects the dissociation rate of the drug, the association rate of VX-770 to the channels can be assessed by measuring the time constant of the current rising phase (τ_{on}) upon the application of VX-770. Here, we report and compare τ_{on} and τ_{off} only, instead of using these numbers as inputs to calculate the theoretical K_d, because we have no evidence for a simple bimolecular reaction between CFTR and VX-770 (or GLPG1837) especially in light of the likelihood that binding occurs in the interface between lipid bilayer and the protein (see Discussion). Fig. 8 B shows that D924N-CFTR not only accelerates the current decay upon removal of VX-770 but also shows a slower rising phase upon the application of VX-770 than WT-CFTR, further strengthening the conclusion of a lower affinity for VX-770. On the other hand, the τ_{on} values for N1138L/G551D- and S1141K/G551D-CFTR do not differ from the τ_{on} for G551D-CFTR (Fig. 8 D). As a negative control, the same experiments were performed on S182A- and S263A-CFTR. Fig. S3 shows that neither τ_{on} nor τ_{off} of VX-770 were affected by these mutations in site IV.

Similar relaxation analysis was performed to test the changes in the affinity for VX-770 by mutations in site II_N. In Fig. 9 A, alanine substitution at Y304, which drastically decreases the affinity for GLPG1837 (Fig. 6), reduces τ_{off} to 13 s (vs. ~360 s for WT-CFTR), suggesting a faster dissociation rate or off rate. In addition, the current rise upon application of VX-770 for Y304A-CFTR is visibly slower than that of WT channels (Fig. 9 A), with a τ_{on} prolonged to 41 s (vs. ~6.7 s for WT-CFTR). Similarly, Fig. 9 B shows an accelerated relaxation upon removal of VX-770 with F312A-CFTR. Fig. 9 C and Table 1 summarize the τ_{on} of VX-770 for site II_N mutants and the significant shortening of the τ_{off} of VX-770 for F236A-, Y304A-, and F312A-CFTR. These results support the proposition that amino acids in both site I and site II_N that interact with GLPG1837 also play important roles in the binding of VX-770. These data shown in Figs. 2, 3, 6, and 7 for GLPG1837 and Figs. 8 and 9 for VX-770 also reaffirm our previous conclusion that GLPG1837 and VX-770 may share a common binding site (Yeh et al., 2017).

In conclusion, our data support the notion that two CFTR potentiators, GLPG1837 and VX-770, share a common binding site and that two specific loci, site I and site II_N, initially identified by molecular docking, may serve as their molecular target sites in the CFTR protein.

Discussion

In this study, we combined in silico docking and the patch-clamp functional assay to identify the molecular target sites for CFTR potentiators GLPG1837 and VX-770, which were previously
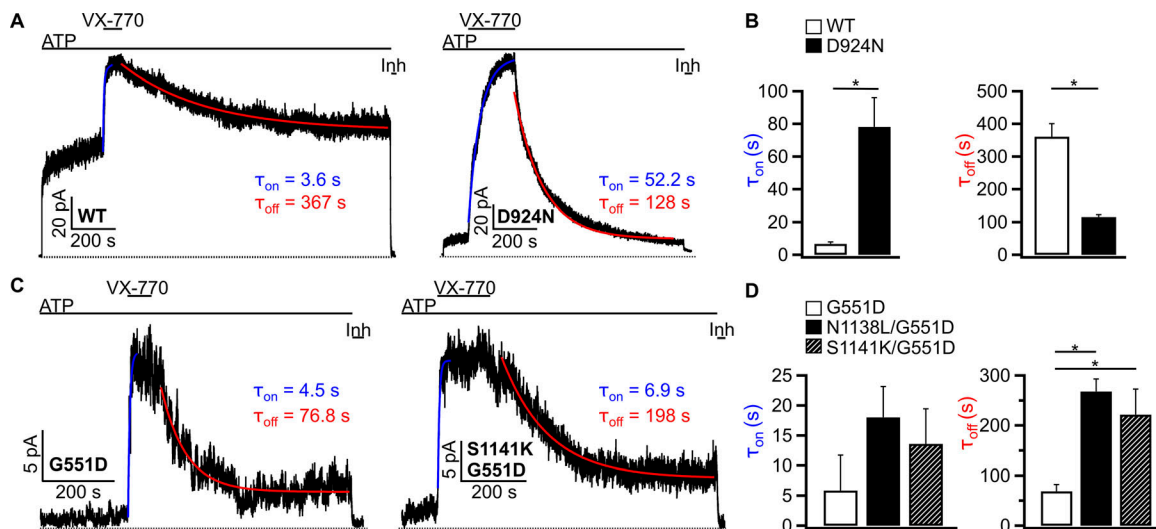
Figure 8. **Effects of mutations in site I on the apparent association and dissociation of VX-770. (A)** Prolonged current rising in response to VX-770 and shortening of the relaxation time course upon removal of VX-770 in D924N-CFTR. After the currents achieved steady state in the presence of 2 mM ATP, an application of 200 nM VX-770 increased the activity of WT-CFTR (left) and D924N-CFTR (right). The current rising phase (blue curve) and the current decay phase (red curve) were fitted with a single-exponential function, yielding the respective time constants, τ_{on} and τ_{off}. **(B)** Comparison of the time constants for the apparent association (τ_{on}) and dissociation (τ_{off}) of VX-770 in WT- and D924N-CFTR. τ_{on}: 6.7 ± 1.2 s (WT); 78.2 ± 18.0 s (D924N). τ_{off}: 361 ± 39 s (WT); 115 ± 7 s (D924N). *, P < 0.05. n = 3 for WT and n = 4 for D924N. **(C)** Representative recordings of G551D- (left) and S1141K/G551D-CFTR (right) showing the exponential current rising/decay upon application/washout of VX-770. **(D)** Prolonged relaxation time constants upon removal of VX-770 in N1138L/G551D- and S1141K/G551D-CFTR. τ_{off}: 68 ± 14 s (G551D), 268 ± 25 s (N1138L/G551D), and 221 ± 50 s (S1141K/G551D). n = 3. *, P < 0.05 (ANOVA followed by Dunnett test). However, changes in the apparent association time constant did not reach a statistically significant level. τ_{on}: 5.9 ± 2.4 s (G551D), 18 ± 5 s (N1138L/G551D), and 14 ± 6 s (S1141K/G551D). Error bars represent SEM.

shown to share a common binding site (Yeh et al., 2017). We provided evidence that two loci at the interface of CFTR's two TMDs, site I (D924, N1138, and S1141) and site II_N (F229, F236, Y304, F312, and F931), are likely to be the binding sites where GLPG1837 and VX-770 exert their function as potentiators. In this section, we will first discuss the intrinsic limitations of the techniques used in the current study, including homology model, molecular docking, and the functional assay using mutants as the main tool. Next, we will delve into more detailed discussion on the complexity in interpreting affinity and efficacy in the context of the state-dependent binding and seek a possible yet imperfect solution to untangle the convoluted relationship between drug binding and channel gating. We will then provide a more in-depth analysis of the pros and cons for each of the identified binding sites for GLGP1837 and VX-770. Finally, we will speculate on the implications of our results on structure-based drug design, and discuss translational significance based on our current understanding of drug effects on patients carrying pathogenic mutations with gating defects.

Limitations of homology modeling, molecular docking, and the functional assay of CFTR using mutation as a tool

It is imperative to realize that the chemical interactions between the potentiators and their targets, which determine their affinity and efficacy, are dynamic as the channel itself usually undergoes multiple conformational changes (Colquhoun, 1998). To hunt for the binding sites, we first need to ask which conformation of the channel is a better starting point. As CFTR is a phosphorylation-activated and ATP-gated channel, the ideal structure would be a

phosphorylated and ATP-bound open CFTR. Since this study started at a time when the corresponding hCFTR structure was unavailable, we employed homology modeling using the cryo-EM structure of zCFTR as a template. Although human and zCFTR share 55% sequence identity that ensures the current modeling techniques could achieve reliable prediction accuracy (Marti-Renom et al., 2003), the possible side-chain rotameric orientations of every amino acid inevitably result in significant uncertainties. This issue is particularly critical, as the drug–protein interaction is highly sensitive to the local amino acid positioning in the binding sites. The fact that our docking software failed to identify site II_N in the homology model because the side chain of residue F931 in the modeled structure obstructs this binding pocket bespeaks this very point.

Although the problem of homology modeling was solved by the timely atomic structure of hCFTR, docking simulation bears its own limitations. First, the computer program allows the drugs to assume different orientations but treats the protein as a rigid body with immobile amino acid side chains. However, it is unrealistic to assume that the amino acids are positioned at the exact location without dynamic changes upon drug binding. For example, according to the induced-fit model, binding of a ligand could cause considerable changes in the shape of its binding site (Koshland, 1958). Thus, the docking software–calculated free energy of interaction between the ligand and its target may not represent the actual condition where the target could adjust to better interact with the ligand. Furthermore, the lipid bilayer is not considered in current docking. The docking simulation assigned a better (i.e., more negative) score to site I than site II_N
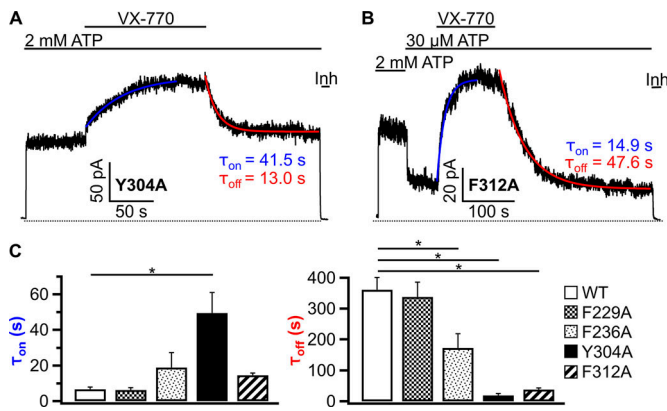
Figure 9. **Apparent association and dissociation rates of VX-770 in site II_N mutants. (A and B)** Macroscopic current traces of Y304A-CFTR (A) and F312A-CFTR (B) in response to application and removal of 200 nM VX-770. The time course of current rise (blue curve, τ_{on}) and current decline (red curve, τ_{off}) were fitted with a single-exponential function. The experiment with F312A-CFTR was performed at 30 µM ATP to adjust its P_o to the level comparable to WT-CFTR (see Fig. 7 for details). CFTR$_{Inh}$-172 (Inh) was applied to attain the baseline. **(C)** Summary of the time constants for the apparent association and dissociation of VX-770. While only Y304A slows down the current rise in response to VX-770, the relaxation time constants for the dissociation of VX-770 are decreased by F236A, Y304A, and F312A mutations. τ_{on}: 6.7 ± 1.2 s (WT); 6.2 ± 1.3 s (F229A); 19 ± 8 s (F236A); 49 ± 11 s (Y304A); 15 ± 1 s (F312A). τ_{off}: 361 ± 39 s (WT); 338 ± 49 s (F229A); 173 ± 45 s (F236A); 18 ± 6 s (Y304A); 38 ± 5 s (F312A). $n = 3$ for WT, F229A, and F312A. $n = 4$ for F236A and Y304A. *, $P < 0.05$ (ANOVA followed by Dunnett test). Error bars represent SEM.

without taking into account the possible roles their distinct local environments may play. For example, while site I resides close to the aqueous permeation pathway, site II_N, located on the lateral surface of CFTR's TMDs, likely makes direct contact with the lipid bilayer. The affinity for site II_N may in fact be greater than site I in a physiological condition due to a more favorable partition of hydrophobic compounds such as GLPG1837 and VX-770 into the lipid phase. In fact, this lipid–protein interface may also account for the observation that alanine substitution of F229 or F236 fails to affect the EC$_{50}$ of GLPG1837 (Fig. 6 B), as the membrane lipids may fill the void and compensate for the loss of binding energy in F229A and F236A. Although what have been discussed here are of a more speculative nature, they highlight the potential limitations of the docking approach to identify the binding sites.

Despite these caveats, we recognized that the docking results can serve as a guide in our hunt for the drug binding sites. Once potential binding partners are identified through docking, we can then alter the amino acids involved in binding and measure the effects of the mutations on the sensitivity and efficacy of the drugs of interest. One immediate problem in mutational study is that we cannot exclude the possibility that observed change in the apparent affinity is actually caused by allosteric effects of the mutation rather than by a direct alteration of the binding event. There are at least two scenarios where the word allosteric applies. First, by allosteric, we mean the amino acid being mutated alters the structure of the actual binding site through a long-distance effect. In an effort to minimize this possibility, we

affirm the binding site only when mutations of a majority of the identified residues in one binding site produce large changes in EC$_{50}$ (also see below and Table 1). For example, all three residues in site I (D924, N1138, and S1141) affect affinity for GLPG1837. Furthermore, the observation of side-chain–specific changes in affinity further supports a specific interaction between the referenced amino acid and the ligand. However, as we do not have evidence to prove this scenario wrong, we caution our audience to be aware of this potential caveat.

The second scenario is much more complex and features a classical struggle while studying the structure–activity relationships for ligands and their target receptors. Here, the term allosteric refers to a mechanism in which the protein exists in two different conformations where their affinities for the ligands could differ substantially. As this issue to some extent is model dependent, it deserves a separate section of discussion. Some thermodynamic considerations will be deliberated first in the next section. We will then discuss the complexity in the relationship between ligand binding and channel gating in the context of an allosteric modulation model.

Complexity in interpreting affinity and efficacy of CFTR potentiators

For now, let us take a more literal interpretation of the measured EC$_{50}$ for the K_d of a CFTR potentiator, whose physicochemical meaning can then be expressed in an energetic term: the free energy of binding (ΔG) = $-RT\ln(K_d)$. In a system without other sources of energy input, the differences in free energy change ($\Delta\Delta G$) between a mutant protein and WT protein undergoing this reaction will be $-RT\ln(K_{d(mutant)}/K_{d(WT)})$, which represents the loss or gain of binding energy introduced by the mutation (see Table 1 for details). When we calculated the corresponding $\Delta\Delta G$ for each mutation in the five binding sites, we found that a majority of mutations in site I and II_N introduces a $\Delta\Delta G$ greater than the other mutations in sites II–IV (Table 1). Specifically, the three mutations in site I with the greatest $\Delta\Delta G$ include D924A, N1138L/G551D, and S1141K/G551D, which result in a $\Delta\Delta G$ (absolute value) >5 kJ/mol. In site II_N, mutations on Y304 and F312 change the ΔG by ≥4 kJ/mol. In contrast, mutations in site II, III, and IV cause smaller $\Delta\Delta G$. If we assume each amino acid contributes to the binding of GLPG1837 independently, and therefore the summation of $\Delta\Delta G$ represents the total loss/gain of binding energy, we can safely conclude that sites I and II_N are more likely to be the binding sites than the remaining three sites.

Although the calculation of $\Delta\Delta G$ provides a quantitative way to evaluate and compare the effects of each mutation on the binding of GLPG1837, it is based on a questionable assumption. As binding of a potentiator affects gating of the channel (i.e., increases the P_o), the reciprocity is also valid. According to the idea of a cyclic model featuring energetic coupling between ligand binding and channel gating (Yeh et al., 2017), the apparent affinity depends not only on the absolute values of the closed and open state affinities but also on the distribution of the channel in these states. Thus, the measured EC$_{50}$ of a potentiator lies between the actual affinity for an open channel and that for a closed channel. In other words, the $\Delta\Delta G$ introduced by a mutation could also be attributed to an alteration of the gating
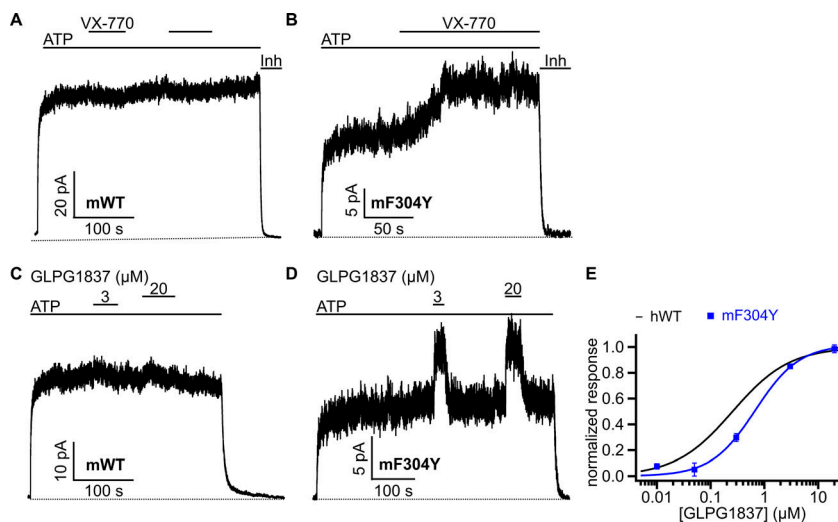
Figure 10. **The response of WT- and F304Y-mCFTR to VX-770 and GLPG1837. (A)** VX-770 fails to potentiate WT-mCFTR. 200 nM VX-770 was applied once the phosphorylated mCFTR channels were opened by 2 mM ATP; 5 µM CFTR$_{inh}$-172 was added at the end of the recording to obtain the baseline. **(B)** Restoring the effect of VX-770 by the F304Y mutation in mCFTR. **(C)** GLPG1837 does not potentiate WT-mCFTR. **(D)** Potentiation of mF304Y-CFTR currents by GLPG1837. **(E)** Dose–response relationships of GLPG1837 for human WT-CFTR (black, from Fig. 2 C) and F304Y-mCFTR (blue). EC$_{50}$ for F304Y-mCFTR: 0.68 ± 0.18 µM. Error bars represent SEM.

equilibrium rather than changing binding (Colquhoun, 1998). Of note, although ATP hydrolysis, by providing an input of free energy into CFTR gating scheme (Csanády et al., 2019), may further complicate the interpretation of mutational effects, the general principle of state-dependent binding for CFTR potentiators likely still holds, since a P_o-dependent EC$_{50}$ has also been demonstrated for G551D-CFTR (Yeh et al., 2017), a mutant with limited capability of ATP hydrolysis (Li et al., 1996; Ramjeesingh et al., 2008).

It is therefore more precautious to state that when a mutation not only shifts the dose–response relationship but also changes the P_o of the channel, it becomes difficult to affirm the role of the residue of interest, since the issue of state-dependent binding discussed above has to be taken into consideration. Ideally, one could find a mutation that changes the dose–response relationship without affecting the P_o, and hence could more confidently attribute the role of the pertinent amino acid to ligand binding. However, the idea of state-dependent binding itself implies that the binding sites must undergo some conformational changes during gating. Thus, mutations meant to affirm the interaction between the ligand and its target very likely also affect gating. Indeed, the mutation D924N in site I decreases the P_o, as the maximal percent increase of currents by GLPG1837 is ~500% (Table 1), implying a $P_o < 0.17$ (1/6). A similar problem is seen with mutation at N1138. N1138Y/G551D-CFTR increases the apparent affinity as well as P_o. The latter is qualitatively attested by the observation that the basal current of N1138Y/G551D-CFTR can easily reach a true "macroscopic" level (i.e., tens of picoamperes), while G551D-CFTR in the same condition rarely generates current greater than a couple of picoamperes. In addition, the efficacy of GLPG1837 is reduced in N1138Y/G551D-CFTR, implying that the basal P_o of this double mutant is likely higher than that of G551D-CFTR. These observations and the resulting complications in data interpretation are perhaps not surprising, because it seems hard to imagine a stationary site I, which is buried in the interface between CFTR's TMD1 and TMD2 and resides close the location of the gate (Gao and Hwang, 2015), during gating transitions.

Site II$_N$ may not be totally immune to this predicament, as the F312A mutation indeed increases the P_o. Nonetheless, as described above, this nonideal condition can at least be amended by assessing the potency of GLPG1837 at a condition with a P_o similar to that of WT-CFTR (Fig. 7). Furthermore, while the Y304A and Y304F mutations show a drastic increase in EC$_{50}$ (>3 µM and 2.28 µM, respectively), the P_o of Y304A-CFTR (0.31) and Y304F-CFTR (0.39) is not very different from that of WT channels (0.4; Fig. S4). Given that these mutations in site II$_N$ barely change P_o but significantly reduce the apparent affinity, we argue that the observed increases of EC$_{50}$ are not caused secondarily to alterations in gating. In summary, although state-dependent binding inevitably complicates the interpretation of our functional data, the fact that our patch-clamp data match well with molecular docking results warrants a more serious consideration of our conclusion that sites I and II$_N$ are the real binding sites for GLPG1837 and VX-770.

Differentiating two identified binding sites

While both site I and site II$_N$ seem to have equivalent supporting evidence for being the binding site for GLPG1837, the effect of GLPG1837 shows no evidence of a cooperativity (Hill coefficient ≈1). More troublesome is the fact that these two sites are both located at the interface between TMD1 and TMD2; they are also situated on the same horizontal plan of the CFTR protein (Figs. 1 A and 5 A). This geographic relationship raises a distinct possibility that any mutations at one site may potentially affect the other. Thus, it is entirely plausible that only one of these two loci is actually the correct binding site. It is known that CFTR orthologues may respond differently to potentiators (Van Goor et al., 2009; Cui et al., 2016). We reason that by comparing the amino acid compositions of sites I and II$_N$ in different species and their response to GLPG1837, we could gain indirect evidence to help differentiate site I and site II$_N$.

As our homology model was built on the zCFTR template, we first compared the amino acid compositions of both sites in zCFTR with those in hCFTR. When the two critical residues in site II$_N$, F312 and Y304, are unaltered at the corresponding positions in zCFTR, the hydrophilic asparagine and serine in site I
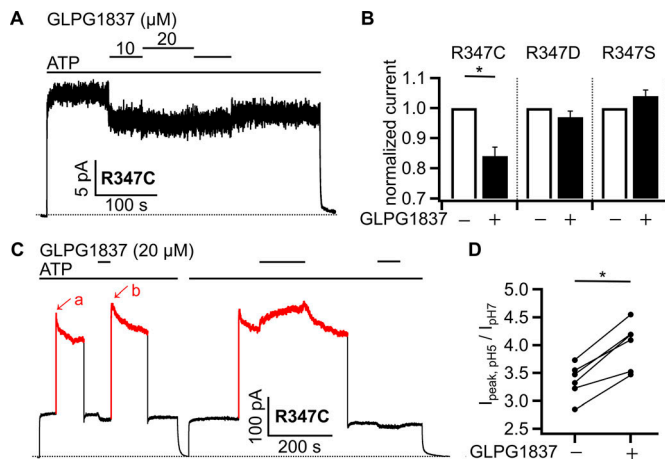
Figure 11. Effects of GLPG1837 on R347C-CFTR at different pH. (A) Inhibitory action of GLPG1837 on R347C-CFTR at pH 7.4. Percent of inhibition: 16 ± 3%, n = 9. **(B)** Loss of potentiation effect of GLPG1837 on R347C/D/S-CFTR. The currents in the presence of GLPG1837 were normalized to the currents in its absence in the same patch. GLPG1837 inhibits R347C-CFTR currents but has no effect on R347D- and R347S-CFTR at pH 7.4. Both the R347D and R347S mutations were introduced to a background construct whose regulatory domain was deleted (ΔR-CFTR). It has been shown that ΔR-CFTR shares similar gating behavior with WT-CFTR without the need for phosphorylation (Bompadre et al., 2005; Sorum et al., 2015, 2017). *, P < 0.05 (paired t test). n = 9, 11, and 4 for R347C-, R347D-, and R347S-CFTR, respectively. **(C)** Opposite effects of GLPG1837 on R347C-CFTR at pH 7.4 and pH 5.5. Macroscopic currents of R347C-CFTR show a biphasic response to pH changed from 7.4 (black) to pH 5.5 (red). The first rising phase (arrow a) results from an increase in the single-channel conductance (Cotten and Welsh, 1999), followed by a slow decay reflecting the decrease in P_o in acidic condition (Cotten and Welsh, 1999). After the currents reached a steady state at pH 5.5, the perfusate was changed back to pH 7.4, and an additional application of GLPG1837 reduced the currents. Following the exposure to GLPG1837 at pH 7.4, the channels were exposed to pH 5.5 perfusate without GLPG1837 (arrow b) and the subsequent current decay is due to combinational effects of acidic condition and the dissociation of GLPG1837. The third segment of the recording highlighted in red shows GLPG1837 effectively potentiates R347C-CFTR at pH 5.5. **(D)** Quantification of the R347C-CFTR currents at pH 5.5 with and without previous exposure to GLPG1837 at pH 7.4. In the absence of GLPG1837, the fold increase in the current magnitude upon changing pH from 7.4 to 5.5 reflects the change in the single channel conductance (peak current at arrow a in C divided by mean current at pH 7.4, $I_{peak, pH5}/I_{pH7}$). With an additional exposure to GLPG1837 at pH 7.4, the fold increase of current upon changing pH (peak current at arrow b in C divided by mean current in ATP at pH 7.4) is consistently greater than that without pretreatment of GLPG1837. The simplest explanation for this result is that GLPG1837 binds to the channel at pH 7.4, but potentiation occurs by the bound ligand at pH 5.5. The straight lines connect data points from the same patch. *, P < 0.05 (paired t test). Error bars represent SEM.

of hCFTR are changed to hydrophobic residues in zCFTR (L1146 and G1149, respectively). The EC50 for GLPG1837 is 3.9 ± 1.7 μM for zCFTR (c.f., 0.26 μM for hCFTR; Fig. S5, A and B). However, neither the single mutation L1146N or G1149S nor the double mutation L1146N/G1149S could restore the affinity (Fig. S5 B). Moreover, it is known that the P_o of zCFTR is much lower than that of hCFTR (Zhang et al., 2018a). Therefore, it is possible that the reduced affinity for GLPG1837 in zCFTR is mostly attributed to the preferential distribution of zCFTR in the closed state.

As zCFTR does not lead to a conclusive answer, we wondered whether a CFTR orthologue that has a distinct site II_N but the

same amino acid composition in site I, as opposed to the case with zCFTR, would provide some insights. Mouse CFTR (mCFTR), which has an identical composition of site I but a different residue in site II_N, serves the purpose (F304 in mCFTR vs. Y304 in hCFTR). Interestingly, neither VX-770 (Fig. 10 A) nor GLPG1837 (Fig. 10 C) can potentiate mCFTR (Van Goor et al., 2009; Bose et al., 2019; but compare Cui and McCarty, 2015). Remarkably, F304Y-mCFTR restores the potentiating effects of both GLPG1837 and VX-770 (Fig. 10, B and D), with an EC50 of 0.68 ± 0.18 μM for GLPG1837. It appears that this position determines an all-or-none effect of the potentiators for mCFTR. Although this line of evidence does not exclude site I or support site II_N to be the correct site, it does suggest that the local structure of site II_N is important for GLPG1837 (or VX-770) to act as a potentiator.

While it is striking that a single mutation in site II_N, F304Y, could restore the action of GLPG1837 and VX-770 in mCFTR, this is not the only position where mutations cause an all-or-none effect of the potentiators during our studies. In fact, mutations at R347 (R347C, R347D, and R347S) in hCFTR, the residue that forms a salt bridge with D924 to stabilize the open channel conformation, abolish the response of hCFTR to GLPG1837 (Fig. 11, A and B). Interestingly, as a well-defined CFTR potentiator, GLPG1837 paradoxically inhibits R347C-CFTR currents by 16 ± 3%. Although it seems puzzling at first glance, the idea of state-dependent binding predicts that the affinity for a ligand to a closed channel relative to an open channel determines whether it is a potentiator or an inhibitor. If the binding of a ligand favors an open (closed) channel, its binding will stabilize the open (closed) state, and the compound will function as a potentiator (inhibitor). Therefore, the reversed action of GLPG1837 on R347C-CFTR could be explained by a reversal of its affinities for the open and closed state. Here, we wonder if this simple idea could also account for the recent report that VX-770 at a micromolar concentration decreases the activity of mCFTR (Bose et al., 2019).

Despite that in the docking simulation R347 is not involved in binding of GLPG1837, its close proximity to site I and interaction with D924 presumably would affect the architecture of this binding site. Cotten and Welsh (1999) have shown that the reduced single-channel conductance of R347C-CFTR could be partially restored by acidification (i.e., lowering pH), implicating a partial reconstruction of the local structure. We thus tested the idea that a similar strategy of lowering pH may also restore the potentiating effect of GLPG17837. As shown in Fig. 11 C, GLPG1837 decreases the currents at pH 7.4 but generates appreciable increase at pH 5.5, supporting our hypothesis. The dual (inhibitory vs. potentiating) actions of GLPG1837 likely result from its binding to a single site with different affinities for GLPG1837 as pH varies (see the Fig. 11, C and D legend for details). While other more complicated scenarios may also explain this observation, the effect of R347C on the action of GLPG1837 suggests that the interaction of R347-D924, which potentially maintains an intact structure of site I, is essential for GLPG1837 to potentiate hCFTR. This idea is tested with R347D/D924R-CFTR, a double mutant in which the side chains of the R347-D924 salt bridge are swapped. Fig.

Yeh et al.
Binding sites for CFTR potentiators

S6 shows that R347D/D924R-CFTR can be potentiated by GLPG1837, supporting the idea that maintaining the local structure of site I is important for the potentiating effect of GLPG1837. The reduced apparent affinity and increased efficacy for GLPG1837 in R347D/D924R-CFTR also corroborate the conclusion that D924 in site 1 plays an important role in gating and/or binding of CFTR potentiators.

Although these additional investigations on zCFTR, mCFTR, and mutations at R347 in hCFTR reveal some interesting results, these data seem to support both sites as the targets for GLPG1837 and VX-770 without providing a firm answer to which is the correct binding site. While a single binding site for these CFTR potentiators is a simpler scenario, multiple binding sites existing in the CFTR protein remain a possibility, and more studies are needed at this juncture.

Implications of structure-based drug design and beyond

Regardless of the pros and cons analyzed above for these two sites, a key feature of them is that both sites are located at the interface of CFTR's two TMDs. This interface likely undergoes conformational changes during the gating motion so that the structures of the binding sites in the closed state would differ from that in the open state, leading to different affinities for CFTR potentiators. For example, the potentiator and the amino acids in the binding site may be closer in an open state, yielding a stronger interaction. It is also possible that after channel opening, some interactions present in the closed state will be lost and other amino acids will impinge onto the potentiator to provide tighter binding. Ultimately, understanding of the specific interactions between the potentiator and its target site in both open and closed channels holds the key for designing compounds with better affinity and efficacy. As the allosteric coupling model between binding and gating suggests, the improvement in affinity relies on stronger binding to both closed and open states, whereas a better efficacy will be achieved by widening the difference between the affinities for each state. In this aspect, knowledge in the structural changes upon channel opening in CFTR's TMDs, particularly in the interface where the proposed binding sites are located, is urgently needed. We believe that the current study in identifying the molecular target sites for CFTR potentiators, together with additional atomic structures of CFTR that could emerge in the near future, should provide a practical guide along the path to realize structure-based drug design for CF therapy.

References

Accurso, F.J., S.M. Rowe, J.P. Clancy, M.P. Boyle, J.M. Dunitz, P.R. Durie, S.D. Sagel, D.B. Hornick, M.W. Konstan, S.H. Donaldson, et al. 2010. Effect of VX-770 in persons with cystic fibrosis and the G551D-CFTR mutation. *N. Engl. J. Med.* 363:1991–2003. https://doi.org/10.1056/NEJMoa0909825

Aleksandrov, A.A., L. Aleksandrov, and J.R. Riordan. 2002. Nucleoside triphosphate pentose ring impact on CFTR gating and hydrolysis. *FEBS Lett.* 518:183–188. https://doi.org/10.1016/S0014-5793(02)02698-4

Bear, C.E., C.H. Li, N. Kartner, R.J. Bridges, T.J. Jensen, M. Ramjeesingh, and J.R. Riordan. 1992. Purification and functional reconstitution of the

cystic fibrosis transmembrane conductance regulator (CFTR). *Cell.* 68:809–818. https://doi.org/10.1016/0092-8674(92)90155-6

Berman, H.M., J. Westbrook, Z. Feng, G. Gilliland, T.N. Bhat, H. Weissig, I.N. Shindyalov, and P.E. Bourne. 2000. The Protein Data Bank. *Nucleic Acids Res.* 28:235–242. https://doi.org/10.1093/nar/28.1.235

Bompadre, S.G., T. Ai, J.H. Cho, X. Wang, Y. Sohma, M. Li, and T.C. Hwang. 2005. CFTR gating I: Characterization of the ATP-dependent gating of a phosphorylation-independent CFTR channel (DeltaR-CFTR). *J. Gen. Physiol.* 125:361–375. https://doi.org/10.1085/jgp.200409227

Bompadre, S.G., Y. Sohma, M. Li, and T.C. Hwang. 2007. G551D and G1349D, two CF-associated mutations in the signature sequences of CFTR, exhibit distinct gating defects. *J. Gen. Physiol.* 129:285–298. https://doi.org/10.1085/jgp.200609667

Bose, S.J., M.J.C. Bijvelds, Y. Wang, J. Liu, Z. Cai, A.G.M. Bot, H.R. de Jonge, and D.N. Sheppard. 2019. Differential thermostability and response to cystic fibrosis transmembrane conductance regulator (CFTR) potentiators of human and mouse F508del-CFTR. *Am. J. Physiol. Lung Cell. Mol. Physiol.* https://doi.org/10.1152/ajplung.00034.2019. https://doi.org/10.1152/ajplung.00034.2019

Byrnes, L.J., Y. Xu, X. Qiu, J.D. Hall, and G.M. West. 2018. Sites associated with Kalydeco binding on human Cystic Fibrosis Transmembrane Conductance Regulator revealed by Hydrogen/Deuterium Exchange. *Sci. Rep.* 8:4664. https://doi.org/10.1038/s41598-018-22959-6

Cai, Z., A. Taddei, and D.N. Sheppard. 2006. Differential sensitivity of the cystic fibrosis (CF)-associated mutants G551D and G1349D to potentiators of the cystic fibrosis transmembrane conductance regulator (CFTR) Cl- channel. *J. Biol. Chem.* 281:1970–1977. https://doi.org/10.1074/jbc.M510576200

Cholon, D.M., N.L. Quinney, M.L. Fulcher, C.R. Esther Jr., J. Das, N.V. Dokholyan, S.H. Randell, R.C. Boucher, and M. Gentzsch. 2014. Potentiator ivacaftor abrogates pharmacological correction of ΔF508 CFTR in cystic fibrosis. *Sci. Transl. Med.* 6:246ra96. https://doi.org/10.1126/scitranslmed.3008680

Colquhoun, D. 1998. Binding, gating, affinity and efficacy: the interpretation of structure-activity relationships for agonists and of the effects of mutating receptors. *Br. J. Pharmacol.* 125:924–947. https://doi.org/10.1038/sj.bjp.0702164

Cotten, J.F., and M.J. Welsh. 1999. Cystic fibrosis-associated mutations at arginine 347 alter the pore architecture of CFTR. Evidence for disruption of a salt bridge. *J. Biol. Chem.* 274:5429–5435. https://doi.org/10.1074/jbc.274.9.5429

Csanády, L. 2000. Rapid kinetic analysis of multichannel records by a simultaneous fit to all dwell-time histograms. *Biophys. J.* 78:785–799. https://doi.org/10.1016/S0006-3495(00)76636-7

Csanády, L., and B. Töröcsik. 2014. Structure-activity analysis of a CFTR channel potentiator: Distinct molecular parts underlie dual gating effects. *J. Gen. Physiol.* 144:321–336. https://doi.org/10.1085/jgp.201411246

Csanády, L., P. Vergani, and D.C. Gadsby. 2019. Structure, Gating, and Regulation of the CFTR Anion Channel. *Physiol. Rev.* 99:707–738. https://doi.org/10.1152/physrev.00007.2018

Cui, G., and N.A. McCarty. 2015. Murine and human CFTR exhibit different sensitivities to CFTR potentiators. *Am. J. Physiol. Lung Cell. Mol. Physiol.* 309:L687–L699. https://doi.org/10.1152/ajplung.00181.2015

Cui, G., N. Khazanov, B.B. Stauffer, D.T. Infield, B.R. Imhoff, H. Senderowitz, and N.A. McCarty. 2016. Potentiators exert distinct effects on human, murine, and Xenopus CFTR. *Am. J. Physiol. Lung Cell. Mol. Physiol.* 311:L192–L207.

Cui, L., L. Aleksandrov, Y.-X. Hou, M. Gentzsch, J.-H. Chen, J.R. Riordan, and A.A. Aleksandrov. 2006. The role of cystic fibrosis transmembrane conductance regulator phenylalanine 508 side chain in ion channel gating. *J. Physiol.* 572:347–358. https://doi.org/10.1113/jphysiol.2005.099457

Dalemans, W., P. Barbry, G. Champigny, S. Jallat, K. Dott, D. Dreyer, R.G. Crystal, A. Pavirani, J.P. Lecocq, and M. Lazdunski. 1991. Altered chloride ion channel kinetics associated with the delta F508 cystic fibrosis mutation. *Nature.* 354:526–528. https://doi.org/10.1038/354526a0

Davies, J.C., S.M. Moskowitz, C. Brown, A. Horsley, M.A. Mall, E.F. McKone, B.J. Plant, D. Prais, B.W. Ramsey, J.L. Taylor-Cousar, et al. VX16-659-101 Study Group. 2018. VX-659-Tezacaftor-Ivacaftor in Patients with Cystic Fibrosis and One or Two Phe508del Alleles. *N. Engl. J. Med.* 379:1599–1611. https://doi.org/10.1056/NEJMoa1807119

Eckford, P.D.W., C. Li, M. Ramjeesingh, and C.E. Bear. 2012. Cystic fibrosis transmembrane conductance regulator (CFTR) potentiator VX-770 (ivacaftor) opens the defective channel gate of mutant CFTR in a phosphorylation-dependent but ATP-independent manner. *J. Biol. Chem.* 287:36639–36649. https://doi.org/10.1074/jbc.M112.393637

Fiser, A., R.K.G. Do, and A. Šali. 2000. Modeling of loops in protein structures. *Protein Sci.* 9:1753–1773. https://doi.org/10.1110/ps.9.9.1753

Forli, S., R. Huey, M.E. Pique, M.F. Sanner, D.S. Goodsell, and A.J. Olson. 2016. Computational protein-ligand docking and virtual drug screening with the AutoDock suite. *Nat. Protoc.* 11:905–919. https://doi.org/10.1038/nprot.2016.051

Gadsby, D.C., P. Vergani, and L. Csanády. 2006. The ABC protein turned chloride channel whose failure causes cystic fibrosis. *Nature.* 440:477–483. https://doi.org/10.1038/nature04712

Gaieb, Z., C.D. Parks, M. Chiu, H. Yang, C. Shao, W.P. Walters, M.H. Lambert, N. Nevins, S.D. Bembenek, M.K. Ameriks, et al. 2019. D3R Grand Challenge 3: blind prediction of protein-ligand poses and affinity rankings. *J. Comput. Aided Mol. Des.* 33:1–18. https://doi.org/10.1007/s10822-018-0180-4

Gao, X., and T.C. Hwang. 2015. Localizing a gate in CFTR. *Proc. Natl. Acad. Sci. USA.* 112:2461–2466. https://doi.org/10.1073/pnas.1420676112

Grinter, S.Z., and X. Zou. 2014. Challenges, applications, and recent advances of protein-ligand docking in structure-based drug design. *Molecules.* 19:10150–10176. https://doi.org/10.3390/molecules190710150

Hadida, S., F. Van Goor, J. Zhou, V. Arumugam, J. McCartney, A. Hazlewood, C. Decker, P. Negulescu, and P.D.J. Grootenhuis. 2014. Discovery of N-(2,4-di-tert-butyl-5-hydroxyphenyl)-4-oxo-1,4-dihydroquinoline-3-carboxamide (VX-770, ivacaftor), a potent and orally bioavailable CFTR potentiator. *J. Med. Chem.* 57:9776–9795. https://doi.org/10.1021/jm5012808

Hanwell, M.D., D.E. Curtis, D.C. Lonie, T. Vandermeersch, E. Zurek, and G.R. Hutchison. 2012. Avogadro: an advanced semantic chemical editor, visualization, and analysis platform. *J. Cheminform.* 4:17. https://doi.org/10.1186/1758-2946-4-17

Hwang, T.C., and D.N. Sheppard. 1999. Molecular pharmacology of the CFTR Cl- channel. *Trends Pharmacol. Sci.* 20:448–453. https://doi.org/10.1016/S0165-6147(99)01386-3

Hwang, T.C., and D.N. Sheppard. 2009. Gating of the CFTR Cl- channel by ATP-driven nucleotide-binding domain dimerisation. *J. Physiol.* 587:2151–2161. https://doi.org/10.1113/jphysiol.2009.171595

Hwang, T.C., F. Wang, I.C. Yang, and W.W. Reenstra. 1997. Genistein potentiates wild-type and delta F508-CFTR channel activity. *Am. J. Physiol.* 273:C988–C998. https://doi.org/10.1152/ajpcell.1997.273.3.C988

Hwang, T.C., J.T. Yeh, J. Zhang, Y.C. Yu, H.I. Yeh, and S. Destefano. 2018. Structural mechanisms of CFTR function and dysfunction. *J. Gen. Physiol.* 150:539–570.

Jih, K.Y., and T.C. Hwang. 2013. Vx-770 potentiates CFTR function by promoting decoupling between the gating cycle and ATP hydrolysis cycle. *Proc. Natl. Acad. Sci. USA.* 110:4404–4409. https://doi.org/10.1073/pnas.1215982110

Jih, K.Y., W.Y. Lin, Y. Sohma, and T.C. Hwang. 2017. CFTR potentiators: from bench to bedside. *Curr. Opin. Pharmacol.* 34:98–104. https://doi.org/10.1016/j.coph.2017.09.015

Koshland, D.E. 1958. Application of a Theory of Enzyme Specificity to Protein Synthesis. *Proc. Natl. Acad. Sci. USA.* 44:98–104. https://doi.org/10.1073/pnas.44.2.98

Li, C., M. Ramjeesingh, W. Wang, E. Garami, M. Hewryk, D. Lee, J.M. Rommens, K. Galley, and C.E. Bear. 1996. ATPase activity of the cystic fibrosis transmembrane conductance regulator. *J. Biol. Chem.* 271:28463–28468. https://doi.org/10.1074/jbc.271.45.28463

Lin, W.Y., K.Y. Jih, and T.C. Hwang. 2014. A single amino acid substitution in CFTR converts ATP to an inhibitory ligand. *J. Gen. Physiol.* 144:311–320. https://doi.org/10.1085/jgp.201411247

Lin, W.Y., Y. Sohma, and T.C. Hwang. 2016. Synergistic Potentiation of Cystic Fibrosis Transmembrane Conductance Regulator Gating by Two Chemically Distinct Potentiators, Ivacaftor (VX-770) and 5-Nitro-2-(3-Phenylpropylamino) Benzoate. *Mol. Pharmacol.* 90:275–285. https://doi.org/10.1124/mol.116.104570

Liu, F., Z. Zhang, L. Csanády, D.C. Gadsby, and J. Chen. 2017. Molecular Structure of the Human CFTR Ion Channel. *Cell.* 169:85–95.e8. https://doi.org/10.1016/j.cell.2017.02.024

Marti-Renom, M.A., A. Fiser, M.S. Madhusudhan, B. John, A.C. Stuart, N. Eswar, U. Pieper, M.-Y. Shen, and A. Sali. 2003. Modeling protein structure from its sequence. *In* Current Protocols in Bioinformatics. A.D. Baxevanis, editor. John Wiley & Sons, New York. pp. 5.1.1–5.1.32.

Martí-Renom, M.A., A.C. Stuart, A. Fiser, R. Sánchez, F. Melo, and A. Sali. 2000. Comparative protein structure modeling of genes and genomes. *Annu. Rev. Biophys. Biomol. Struct.* 29:291–325. https://doi.org/10.1146/annurev.biophys.29.1.291

Miki, H., Z. Zhou, M. Li, T.C. Hwang, and S.G. Bompadre. 2010. Potentiation of disease-associated cystic fibrosis transmembrane conductance regulator mutants by hydrolyzable ATP analogs. *J. Biol. Chem.* 285: 19967–19975. https://doi.org/10.1074/jbc.M109.092684

Ostedgaard, L.S., O. Baldursson, and M.J. Welsh. 2001. Regulation of the cystic fibrosis transmembrane conductance regulator Cl- channel by its R domain. *J. Biol. Chem.* 276:7689–7692. https://doi.org/10.1074/jbc.R100001200

Quinton, P.M., and M.M. Reddy. 1991. Regulation of absorption in the human sweat duct. *Adv. Exp. Med. Biol.* 290:159–170, discussion :170–172. https://doi.org/10.1007/978-1-4684-5934-0_17

Ramjeesingh, M., F. Ugwu, F.L. Stratford, L.J. Huan, C. Li, and C.E. Bear. 2008. The intact CFTR protein mediates ATPase rather than adenylate kinase activity. *Biochem. J.* 412:315–321. https://doi.org/10.1042/BJ20071719

Riordan, J.R., J.M. Rommens, B. Kerem, N. Alon, R. Rozmahel, Z. Grzelczak, J. Zielenski, S. Lok, N. Plavsic, J.L. Chou, et al. 1989. Identification of the cystic fibrosis gene: cloning and characterization of complementary DNA. *Science.* 245:1066–1073. https://doi.org/10.1126/science.2475911

Rowe, S.M., S. Miller, and E.J. Sorscher. 2005. Cystic fibrosis. *N. Engl. J. Med.* 352:1992–2001. https://doi.org/10.1056/NEJMra043184

Šali, A., and T.L. Blundell. 1993. Comparative protein modelling by satisfaction of spatial restraints. *J. Mol. Biol.* 234:779–815. https://doi.org/10.1006/jmbi.1993.1626

Sorum, B., D. Czégé, and L. Csanády. 2015. Timing of CFTR pore opening and structure of its transition state. *Cell.* 163:724–733. https://doi.org/10.1016/j.cell.2015.09.052

Sorum, B., B. Töröcsik, and L. Csanády. 2017. Asymmetry of movements in CFTR's two ATP sites during pore opening serves their distinct functions. *eLife.* 6:e29013. https://doi.org/10.7554/eLife.29013

Trott, O., and A.J. Olson. 2010. AutoDock Vina: improving the speed and accuracy of docking with a new scoring function, efficient optimization, and multithreading. *J. Comput. Chem.* 31:455–461.

Tsai, M.F., H. Shimizu, Y. Sohma, M. Li, and T.C. Hwang. 2009. State-dependent modulation of CFTR gating by pyrophosphate. *J. Gen. Physiol.* 133:405–419. https://doi.org/10.1085/jgp.200810186

Van der Plas, S.E., H. Kelgtermans, T. De Munck, S.L.X. Martina, S. Dropsit, E. Quinton, A. De Blieck, C. Joannesse, L. Tomaskovic, M. Jans, et al. 2018. Discovery of N-(3-Carbamoyl-5,5,7,7-tetramethyl-5,7-dihydro-4H-thieno[2,3-c]pyran-2-yl)-lH-pyrazole-5-carboxamide (GLPG1837), a Novel Potentiator Which Can Open Class III Mutant Cystic Fibrosis Transmembrane Conductance Regulator (CFTR) Channels to a High Extent. *J. Med. Chem.* 61:1425–1435. https://doi.org/10.1021/acs.jmedchem.7b01288

Van Goor, F., S. Hadida, P.D. Grootenhuis, B. Burton, D. Cao, T. Neuberger, A. Turnbull, A. Singh, J. Joubran, A. Hazlewood, et al. 2009. Rescue of CF airway epithelial cell function in vitro by a CFTR potentiator, VX-770. *Proc. Natl. Acad. Sci. USA.* 106:18825–18830. https://doi.org/10.1073/pnas.0904709106

Van Goor, F., S. Hadida, P.D. Grootenhuis, B. Burton, J.H. Stack, K.S. Straley, C.J. Decker, M. Miller, J. McCartney, E.R. Olson, et al. 2011. Correction of the F508del-CFTR protein processing defect in vitro by the investigational drug VX-809. *Proc. Natl. Acad. Sci. USA.* 108:18843–18848. https://doi.org/10.1073/pnas.1105787108

Van Goor, F., H. Yu, B. Burton, and B.J. Hoffman. 2014. Effect of ivacaftor on CFTR forms with missense mutations associated with defects in protein processing or function. *J. Cyst. Fibros.* 13:29–36. https://doi.org/10.1016/j.jcf.2013.06.008

Veit, G., R.G. Avramescu, D. Perdomo, P.-W. Phuan, M. Bagdany, P.M. Apaja, F. Borot, D. Szollosi, Y.-S. Wu, W.E. Finkbeiner, et al. 2014. Some gating potentiators, including VX-770, diminish ΔF508-CFTR functional expression. *Sci. Transl. Med.* 6:246ra297.

Veit, G., R.G. Avramescu, A.N. Chiang, S.A. Houck, Z. Cai, K.W. Peters, J.S. Hong, H.B. Pollard, W.B. Guggino, W.E. Balch, et al. 2016. From CFTR biology toward combinatorial pharmacotherapy: expanded classification of cystic fibrosis mutations. *Mol. Biol. Cell.* 27:424–433. https://doi.org/10.1091/mbc.e14-04-0935

Vergani, P., A.C. Nairn, and D.C. Gadsby. 2003. On the mechanism of MgATP-dependent gating of CFTR Cl- channels. *J. Gen. Physiol.* 121:17–36. https://doi.org/10.1085/jgp.20028673

Vergani, P., S.W. Lockless, A.C. Nairn, and D.C. Gadsby. 2005. CFTR channel opening by ATP-driven tight dimerization of its nucleotide-binding domains. *Nature.* 433:876–880. https://doi.org/10.1038/nature03313

Wang, Y., J.A. Wrennall, Z. Cai, H. Li, and D.N. Sheppard. 2014. Understanding how cystic fibrosis mutations disrupt CFTR function: from single molecules to animal models. *Int. J. Biochem. Cell Biol.* 52:47–57. https://doi.org/10.1016/j.biocel.2014.04.001

Webb, B., and A. Sali. 2016. Comparative Protein Structure Modeling Using MODELLER. *Curr. Protoc. Bioinformatics.*54:5.6.1–5.6.37.

Yan, C., S.Z. Grinter, B.R. Merideth, Z. Ma, and X. Zou. 2016. Iterative Knowledge-Based Scoring Functions Derived from Rigid and Flexible Decoy Structures: Evaluation with the 2013 and 2014 CSAR Benchmarks. *J. Chem. Inf. Model.* 56:1013–1021. https://doi.org/10.1021/acs.jcim.5b00504

Yeh, H.I., J.T. Yeh, and T.C. Hwang. 2015. Modulation of CFTR gating by permeant ions. *J. Gen. Physiol.* 145:47–60. https://doi.org/10.1085/jgp.201411272

Yeh, H.I., Y. Sohma, K. Conrath, and T.C. Hwang. 2017. A common mechanism for CFTR potentiators. *J. Gen. Physiol.* 149:1105–1118. https://doi.org/10.1085/jgp.201711886

Yu, H., B. Burton, C.J. Huang, J. Worley, D. Cao, J.P. Johnson Jr., A. Urrutia, J. Joubran, S. Seepersaud, K. Sussky, et al. 2012. Ivacaftor potentiation of multiple CFTR channels with gating mutations. *J. Cyst. Fibros.* 11: 237–245. https://doi.org/10.1016/j.jcf.2011.12.005

Zhang, Z., and J. Chen. 2016. Atomic Structure of the Cystic Fibrosis Transmembrane Conductance Regulator. *Cell.* 167:1586–1597.

Zhang, J., Y.C. Yu, J.T. Yeh, and T.C. Hwang. 2018a. Functional characterization reveals that zebrafish CFTR prefers to occupy closed channel conformations. *PLoS One.* 13:e0209862. https://doi.org/10.1371/journal.pone.0209862

Zhang, Z., F. Liu, and J. Chen. 2017. Conformational Changes of CFTR upon Phosphorylation and ATP Binding. *Cell.* 170:483–491.e8. https://doi.org/10.1016/j.cell.2017.06.041

Zhang, Z., F. Liu, and J. Chen. 2018b. Molecular structure of the ATP-bound, phosphorylated human CFTR. *Proc. Natl. Acad. Sci. USA.* 115:12757–12762. https://doi.org/10.1073/pnas.1815287115

Zhou, Z., X. Wang, M. Li, Y. Sohma, X. Zou, and T.C. Hwang. 2005. High affinity ATP/ADP analogues as new tools for studying CFTR gating. *J. Physiol.* 569:447–457. https://doi.org/10.1113/jphysiol.2005.095083

Zhou, Z., X. Wang, H.Y. Liu, X. Zou, M. Li, and T.C. Hwang. 2006. The two ATP binding sites of cystic fibrosis transmembrane conductance regulator (CFTR) play distinct roles in gating kinetics and energetics. *J. Gen. Physiol.* 128:413–422. https://doi.org/10.1085/jgp.200609622

Zielenski, J., and L.C. Tsui. 1995. Cystic fibrosis: genotypic and phenotypic variations. *Annu. Rev. Genet.* 29:777–807. https://doi.org/10.1146/annurev.ge.29.120195.004021